FABRICATED Bi_2O_3/TiO_2 HETEROJUNCTION NANOCOMPOSITES FOR THE DEGRADATION OF REVERSE OSMOSIS CONCENTRATE

XIANG JIAO

NATIONAL UNIVERSITY OF SINGAPORE

2015

FABRICATED Bi_2O_3/TiO_2 HETEROJUNCTION NANOCOMPOSITES FOR THE DEGRADATION OF REVERSE OSMOSIS CONCENTRATE

XIANG JIAO

(M.Sc., Peking University)

A THESIS SUBMITTED

FOR THE MASTER DEGREE OF SCIENCE

DEPARTMENT OF CHEMISTRY

NATIONAL UNIVERSITY OF SINGAPORE

2015

Declaration

I hereby declare that this thesis is my original work and it has been written by me in its entirety, under the supervision of Professor Li Fong Yau, Sam and Professor Chang Young-Tae, Department of Chemistry, National University of Singapore, between 05/08/2014 and 04/08/2015.

I have duty acknowledged all the sources of information which have been used in the thesis.

This thesis has also not been submitted for any degree in any university previously.

Xiao Jiao	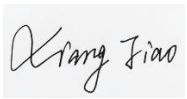	Aug 19, 2015
Name	Signature	Date

Acknowledgements

As my study in NUS will come to an end soon, I am glad to convey my deepest appreciation to all those who have offered me invaluable help. Sincerely thank you all. Special thanks to PUB (Public Utilities Board) for providing the SPORE scholarship to my study in NUS.

Firstly, I would like to present my heartfelt gratefulness to my supervisors, Professor Li Fong Yau, Sam and Professor Chang Young-Tae, for their invaluable instruction, constant encouragement, patience and understanding throughout the whole length of my study in NUS. Thank you for the great help and support. Your rigorous attitude and profound knowledge benefit me so much.

Secondly, I should give my hearty thanks to my mentor Mr. Lin Xuanhao. Thank you for your constant guidance and encouragement. You taught me much knowledge about equipment and professional knowledge. Without your consistent and long term patience, it would be hard for me to complete my project smoothly.

Deeply grateful to everyone in our group. I regard this group as a warm family, members here are so kind like to help each other, and I really appreciate the period we studied together.

I would also extend my heartfelt thanks to all my friends. Especially my roommate for the one year companion in Singapore, we lived like brothers here. I also want to thanks my thesis examiners for all your energy and time you put in reviewing my thesis. Thank you so much for your kindly advice.

Last but not least, I want to thank my parents. Thank you for all the supports, love and understanding. Because of you, I got the reason and motivation of my struggle.

Commencement in NUS is not just mean an ending, it’s also has a meaning of

new start. With all things I gained in my learning and training, I am so powerful to pursue my dreams. I will always bear in mind: Just do it, keep moving!

Xiang Jiao

2015-08-20

National University of Singapore

Table of Contents

Summary V

List of Tables VII

List of Figures VIII

List of Abbreviations X

Chapter 1 Introduction 1

1.1 Background 1

1.2 Wastewater treatment process 1

1.3 Photocatalytic process in wastewater treatment 4

1.4 Properties of TiO_2 photocatalysts 6

1.5 Bismuth based photocatalysts 8

1.6 Heterojunctions 11

Chapter 2 Materials and Methodology 13

2.1 Materials 13

2.2 Methodology 14

2.2.1 Preparation of carbon spheres 14

2.2.2 Preparation of carbon sphere supported TiO_2 17

2.2.3 Fabrication of Bi_2O_3/TiO_2 19

2.3 Characterization 20

2.3.1 Powder X-ray Diffraction 20

2.3.2 BET analysis 23

2.3.3 N_2 sorption porosimetry 24

2.3.4 Scanning electron microscopy 26

2.3.5 UV-vis diffuse reflectance spectroscopy 27

2.2.6 Fluorescence spectroscopy 28

2.3.7 TOC analysis 29

Chapter 3 Results and discussion 30

3.1 XRD analysis 30

3.2 FT-IR analysis 33

3.3 BET analysis 35

3.4 SEM analysis 37

3.5 UV–visible DRS analysis 39

Chapter 4 Photo-catalysis Reaction to Degrade ROC 42

4.1 Photocatalytic experiments 42

4.2 fluorescent intensity 43

4.3 Comparison of photocatalytic activities 44

Chapter 5 Conclusion and future work 48

Summary

With the increase demand for clean water, there are more and more research focused on the development of materials and processes for water treatment recently.

TiO_2 has been widely used in environmental decontamination field because of its wide band gap. Through TiO_2 photo-catalysis process, most of pollutants such as organic compounds can be mineralized to harmless compounds. However, due to the high cost, the application of TiO_2 photo-catalysis treatment has been hindered. At the same time, as the reverse osmosis technology is widely applied in water desalination around the world, it is urgent to find an environmental friendly and economical way to dispose this industry by-product, namely RO concentrates.

In this study, Bi_2O_3/TiO_2 heterojunction nanocomposites synthesized to reduce the cost of this catalyst. A series of Bi_2O_3/TiO_2 heterojunction nanocomposites were synthesized successfully: TiO_2, Bi_2O_3, Bi_2O_3/TiO_2 (Bi-Ti at different atomic ratios were synthesized through direct hydrolysis and hydrothermal method. We made mechanistic studies on characterization of the catalysts we fabricated. We also tested the photo-catalytic activities of these catalysts for organics de-gradation of RO concentrate (ROC) under visible light and UV light, and made TOC analysis, Fluorescence spectroscopy analysis, UV-Vis adsorption spectroscopy analysis and so on.

Our results show that some of the Bi_2O_3/TiO_2 heterojunction nanocomposites catalysts we synthesised to facilitate ROC degradation is environmental friendly and has better efficiency. However more research needs to be done to understand the mechanism to improve the efficiency.

List of Tables

Table 2-1 Details on different fabricated Bi_2O_3/TiO_2 heterojunction.....16

Table 2-2 The dosages of $Bi(NO_3)_3•5H_2O$ and $TiOSO_4•xH_2O$ 17

Table 3-1 Specific surface and pore architecture of Bi_2O_3/TiO_2 composites...37

List of Figures

Figure 1-1 Flow diagrams of several technologies of waste water treatment....3

Figure 2-1 Chematic illustration of the formation of Bi_2O_3/TiO_2 heterojunction 15

Figure 2-2 Synthesized carbon spheres.....17

Figure 2-3 Schematic of photoreactor used in this study.....18

Figure 2-4Synthesized Bi_2O_3/TiO_2 heterojunction nanocomposites 20

Figure 2-5 Schematic diagram of the scattering of x-rays by a crystalline material 22

Figure 3-1 The X-ray powder diffraction patterns of pure α - Bi_2O_3, TiO_2 and Bi_2O_3/TiO_2 photocatalysts.....32

Figure 3-2 FT-IR of Bi_2O_3/TiO_2 heterojunction nanocomposites 35

Figure 3-3 Nitrogen adsorption-desorption isotherms of Bi_2O_3/TiO_2 photocatalysts.....36

Figure 3-4 SEM of Bi_2O_3/TiO_2 photocatalysts 38

Figure 3-5 UV-Visible diffuse reflectance spectra of Bi_2O_3/TiO_2 photocatalysts 40

Figure 4-1 Reaction equipment for ROC reaction.....42

Figure 4-2 Changes in the fluorescent intensity of the RO aqueous solutions under visible light irradiation in the presence of Bi_2O_3/TiO_2. 43

Figure 4-3 Comparison of photocatalytic activities of different Bi_2O_3/TiO_2 NTs

for the photocatalytic decomposition of ROC in water. 46

Figure 4-4 Illustration of formed B-type heterojunction of the Bi_2O_3/TiO_2 photocatalysts. 47

Figure 5-1 Proposed design of multiple heterojunction photocatalysts with both A-type and B-type heterojunctions in the same catalysts. 50

List of Abbreviations

BET Brunauer-Emmett-Teller

XRD X-ray diffraction

FT-IR Fourier transform infrared

UV–visible DRS UV-visible diffuse reflectance spectra

FESEM Field emission scanning electron microscopy

ROC Reverse osmosis concentrate

SPD Spray pyrolysis deposition

TOC Total organic carbon

Chapter 1 Introduction

1.1 Background

As one of the most important resources for human being, water resource play an important part in our world. With the rapid development of industry, there are more and more industries needs a large quantity of water, as a result, there are too much of water discharged from industries contaminated with toxic organic pollutants. With the increasing population of the world and the high level of industrialization, great amounts of organic pollutants, containing industrial chemicals, pesticide remnant, organic waste, dyes, and daily-life waste, have been discharged into the natural water reservoirs (Brillas et al., 2009). Therefore, it is urgent to overcome the water pollution problem.

1.2 Wastewater treatment process

Usually, an ideal waste treatment procedure will completely dispose all the toxic species present in the waste stream without leaving behind any harmful by-products. It should also not be too expensive. Some sewage treatment methods are in practice successfully up to now. Fig.1-1 shows flow diagrams of several technologies of waste water treatment (Wise, 1994). However, each process has its shortcomings. For example, air stripping processes, usually used to treat the volatile organic pollutants for aqueous media, merely transform the pollutants

from water phase to air phase rather than destroy them completely. The adsorption of granular activated carbon (GAC) is a traditional method to remove the organic pollutants from wastewater. In the process of adsorption, the spent carbon must be either incinerated or regenerated, which converts adsorbed pollutants to innocuous by-product. As to the water disinfection and destructive oxidation technologies in water treatment process, ozonation and chlorination are two main methods, however, chlorination based water disinfection process would form potentially toxic disinfection by-products, such as trihalomethanes.

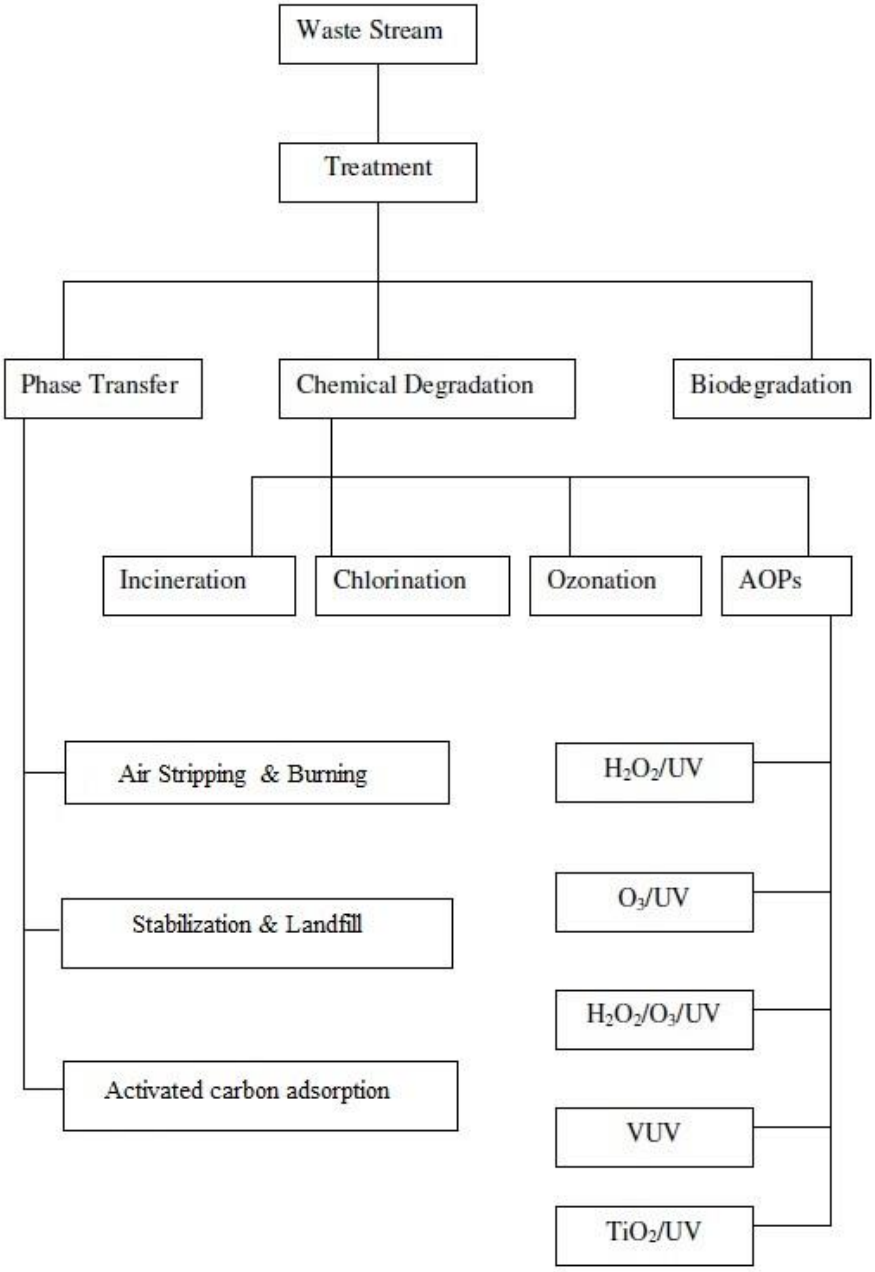

Figure 1-1 Flow diagrams of several technologies of waste water treatment.

Ozonation is considered as a better water treatment process over chlorination as it avoids the formation of disinfection by-products associated with chlorinated organic compounds (Klavarioti et al., 2009). But, recently it has been discovered that ozone can generate cancer-causing agent, and it may cause other hazards.The incineration of organic waste was widely used, but it is not an ideal water treatment process because the incineration of many organic hazardous

compounds can release another toxic components into the air. A relatively new set of technology methods, mentioned as Advanced Oxidation Process (AOPs), developed from research works has been regarded to conquer much limitations of traditional treatment process of wastewater. Generally, AOPs include O_3/UV, H_2O_2/UV, H_2O_2/O_3/UV, vacuum UV and photocatalytic processes using light and semiconductor catalysts (Vogna et al., 2004). Especially, the semiconductor photocatalysis applied to degrade organic pollutants has attracted more and more attention over the last several decades.

1.3 Photocatalytic process in wastewater treatment

In Recent years, there are more and more photochemical or catalytic methods applied have led to progress in procedure of oxidative degradation for organic contaminants dissolved and dispersed in aqueous media. They referred to Advanced Oxidation Processes (AOPs) in general and are considered to be a substitute for conventional water treatment process recently. Among the AOPs, photocatalytic oxidation, due to its many unique features, sensitized by semiconductor photocatalyst such as TiO_2/UV, has attracted much attention in recent years as an alternative for treating water polluted by toxic organic compounds. Photocatalysis differs from other AOPs as it employs very low energy UV-A light, and also reusable catalysts, and it does not need extra oxidants. There are some merits of photocatalysis compared to other conventional methods have been concluded as follows (Andreozzi et al., 2005):

(1) A green technique as the degradation products (carbon dioxide, water and mineral acid) are environmentally harmless.

(2) Almost all organic pollutants in wastewater can be mineralized, such as hydroxyl radical resistant, such as carbon tetrachloride.

(3) There is a low cost process as atmospheric oxygen is used as the only oxidant, and solar light or low energy UV light is used for photocatalyst activation,

(4) Requirement of mild temperature and pressure conditions are usually sufficient.

(5) The photocatalysts are cheap, stable, non-toxic, biologically and chemically inert, insoluble under most conditions and reusable.

A photocatalytic reaction is associated with the irradiation of semiconductor particles, such as titanium dioxide (TiO_2), by UV light which has more energy than the band gap energy of the semiconductor, defining as the energy gap between the valence band and conduction band of a semiconductor. Upon irradiation of the semiconductor by a suitable light, holes and electrons will generate in the semiconductor, and these holes and electrons can oxidize or reduce the adsorbed organic and inorganic compounds (Esplugas et al., 2002). Semiconductor photocatalyst has received more and more attention over the last twenty years because of its intriguing advantages for water purification from Fujishima and Honda's (1972) work on changed water into hydrogen and oxygen using UV irradiated TiO_2 electrode. Ollis and his co-workers (Purdan and Ollis, 1983; Ollis et al., 1984) found the semiconductor photocatalysis as

an emerging water purification technique by their established works using a great deal of organic elements. It was illustrated 1200 references on the subject and included a large list of chemicals that can be treated by photocatalytic process (Pera et al., 2004). In a typical photocatalytic process, the two main factors determine whether the reaction can be successfully carried out or not. They are semiconductor photocatalyst and suitable light resource.

1.4 Properties of TiO_2 photocatalysts

Titanium dioxide (TiO_2), has long been studied for environmental applications, it is commonly regarded as one of the most stable and active photocatalysts (Stepnowski et al., 2005), it has been thought to be low cost and non-toxic nature, and some other advantages made TiO_2 become the most popular catalyst. Therefore, there are tremendous interest rose in TiO_2 with its applications in hydrogen production, decontamination, organic synthesis, disinfection, and so on. It is one of the best semiconductors for sensitizing reaction. However, the wide band gap of TiO_2 (3.0 eV for rutile and 3.2 eV for anatase.) presents a main drawback as only the ultraviolet part of the solar sunlight could be utilized. This is compounded by a high recombination rate for the electron-hole pairs, limiting the quantum yield (Hernandez et al., 2009). The localization of the electron as a Ti^{3+} species was reported to occur with a time scale of about 30 ps and about 90% or even more of the photogenerated electron-hole pairs recombined within 10 ns (Serpone et al., 1995). In solutions, the quantum yield

is less than 1% in photocatalysis by TiO_2.

There are some ways for developing visible-light-active photocatalysts in recent years. One method is the design of photocatalytic materials that can absorb visible light. Recently, many new photocatalytic semiconductors with narrower band gap such as Bi_2O_3 (Zhang et al., 2006), WO_3 (Katsumata et al., 2014; Liew et al., 2014), CdSe (Ho et al., 2006; Frame et al., 2008; Zhu et al., 2013), $BiVO_4$ (Dong et al., 2014; Thalluri et al., 2014; Li et al., 2014; Chala et al., 2014; Xu et al., 2014; Sheng et al., 2014), $Bi_{12}TiO_{20}$ have been developed (Lin et al., 2007; Xu et al., 2007; Zhou et al., 2007; Kim et al., 2010; Hou et al., 2011; Bi et al., 2012; Wei et al 2012; Choi et al., 2004). Fabrication of the wide band gap materials (for example, TiO_2) by doping metal or nonmetal into its crystal structure is also an effective way. A large number of materials have been reported, including Bi doped TiO_2 (Xu et al., 2002; Xin et al., 2005; Li et al., 2009), C doped TiO_2, N doped TiO_2 and others. Since nanoparticles of noble metal, such as Ag, have strong visible light absorption depend on the surface plasmon resonance effect, Ag or Au nanoparticles supported on wide band gap photocatalysts, such as Ag/TiO_2 or Au/TiO_2 were found to be highly efficient photocatalysts under visible light. Another important and effective way is forming heterojunctioned composites between two semiconductors with different band position, which will be introduced in detail here.

1.5 Bismuth based photocatalysts

Bismuth (Bi), is the 83rd element and the heaviest stable element on the periodic table, its atomic mass is 208.980. Bismuth is a relatively rare element (ranking 64th in abundance in the Earth's crust), however, large quantities of bismuth are produced annually as a by-product of copper and tin refining. It is a heavy metal though, bismuth is thought to be safe, as it is noncarcinogenic and non-toxic (Leonard et al., 2002). Bismuth salts are used widely in pharmaceutical products as antacids and in the treatment of peptic ulcers. Most bismuth compounds are non-toxic and relatively easy to be treated (Kudo et al., 1999). With increasing environmental concern, bismuth containing semiconductors have got the attention of many researchers in recent years. As deep valence bands are formed by linear combinations of O_{2p} orbitals, the conduction band (CB) levels of narrow-band-gap oxide semiconductors are usually low, usually relative to the vacuum level). Because of this it is hard to develop visible-light-driven and stable oxide photocatalyst. There is a need to control the valence band (VB) with orbitals of more electro-positive elements than O_{2p} to move the absolute position higher. It has been found that bismuth is a potential substitute as such a valence band control element (Leontie et al., 2002). Recently, great efforts have been devoted to develop bismuth photocatalysts with good activity for water splitting or environmental application, such as Bi_2O_3, $BiVO_4$, $BiFeO_3$, Bi_2WO_6, $NaBiO_3$, $CaBi_2O_4$, $Bi_{12}TiO_{20}$.

There are six polymorphs of Bi_2O_3, i.e. α-Bi_2O_3, β-Bi_2O_3, γ-Bi_2O_3, δ-Bi_2O_3, ε-Bi_2O_3, and ω-Bi_2O_3. Under low temperatures, the stable form is the monoclinic α-Bi_2O_3, while it transforms to the cubic fluorite δ-Bi_2O_3 when heated above 727 ^oC. All the other structures are metastable (Zhou et al., 2009). The band gap of Bi_2O_3 lies between 2.0 and 2.8 eV, depending on the crystalline phase. In the Bi (III) semiconductors, the Bi 6s and O 2p levels hybridize to form the valence band while the conduction band is derived from Bi 6p orbitals (Kudo et al., 1999).

Eberl (Eberl et al., 2008) prepared α-bismuth oxides by three different methods. The direct calcination of salts such as $Bi(NO_3)_3$ $5H_2O$, $BiONO_3$, $(BiO)_2CO_3$ and BiOCl at 500 °C led to powders of poor to moderate photoactivity for the degradation of 4-chlorophenol under visible light (λ > 420 nm). Bismuth oxides formed by precipitation of bismuth and bismuthyl nitrates with NaOH and subsequent calcination gave the highest activity with complete photomineralization of 4-chlorophenol. However, the evolved CO_2 resulted in the formation of bismuth carbonates that could not be removed despite calcination at 500 °C for 1 h. Zhang et al (2006) obtained nanosized Bi_2O_3 of 40-100 nm using polyvinylpyrrolidone (PVP) as surfactant in the synthesis. High-intensity ultrasound treatment caused dehydration of $Bi(OH)_3$ into Bi_2O_3 while the addition of PVP resulted in the formation of granular grains rather than rod-like structures. The resulting nanoparticles degraded 86 % of methyl orange to NO, NO_2 and CO_2 within 100 min using visible light (λ > 400 nm). In

comparison, micron-sized Bi_2O_3 showed lower conversion under similar conditions while TiO_2 (P-25) was inactive. By introducing VO_3^- into the reaction system, Zhou and coworkers successfully synthesized a uniform hierarchical δ-Bi_2O_3, composed of 2D nanosheets intercrossed with each other. This material possessed surface area as high as 72.9 $m^2 \bullet g^{-1}$ and exhibited 10 times higher activity compared to a commercial Bi_2O_3 for the degradation of RhB under visible light irradiation ($\lambda > 400$ nm). Wang et al (2010) prepared Ti-doped β-Bi_2O_3 by a hydrothermal method with subsequent calcination at 400 ^oC and tested it for the photodegradation of indigo carmine, Rhodamine B, and methylene blue under visible-light irradiation. The Ti-doped sample was more resistant to the formation of $(BiO)_2CO_3$ than β- Bi_2O_3 and could be reused. In contrast, even after one run, the undoped β–Bi_2O_3 transformed to predominantly the α-phase (81 %) with the formation of $(BiO)_2CO_3$ (11 %). Interestingly, a 3D flowerlike hierarchical Fe_3O_4@Bi_2O_3 core-shell architecture was reported by Wang et al (2011). They used Bi_2O_3 as the shell, which was formed on the surface of Fe_3O_4 by Ostwald ripening and a self-assembly process. The surface area of this core-shell structure (73.8 $m^2 \bullet g^{-1}$) was much higher than that of commercial Bi_2O_3 (0.368 $m^2 \bullet g^{-1}$), which resulted in a ten times higher activity than commercial Bi_2O_3 particles under visible-light reaction. Furthermore, these photocatalysts can easily be separated by applying an external magnetic field.

1.6 Heterojunctions

Combination of semiconductors is regarded as an effective way to improve the photostimulated electron-hole separation and can effectively inhibits their recombination. The main characteristic of this method is to assemble a heterojunction interface between wide and narrow band gap semiconductors with matching energy band potentials. In this method, electric field assisted transportation of charges from one particle to others through interfaces is favorable for the electron-hole separations in the composite materials, and thus the electron and hole could move to the surface of the semiconductors. When two semiconductors with different energies for their valence and conduction bands are in contact, a heterojunction structure formed. The vectorial transfer of electrons and holes from one semiconductor to the other reduces the intrinsic recombination rate (Augugliaro et al., 2010). This increases the efficiency of the charge-transfer process at the solid-liquid interface. Depending on the band gap of the two components, such structures can be divided into two classes, i.e. only one visible-light-responsive photocatalyst, or two visible-light-responsive photocatalysts. The more research published on this heterojunction system were mostly focused on TiO_2 based photocatalysts, such as WO_3/TiO_2, SiO_2/TiO_2, MgO/TiO_2, Bi_2O_3/TiO_2, $FeTiO_3/TiO_2$ and so on.

Bi_2O_3, with a band gap of 2.8 eV is known as p-type semiconductor, and it has widely been used in gas sensors, optical coatings and solid oxide fuel cells.

Moreover, Bi_2O_3 has proved to be a good photocatalyst for water splitting and pollutant decomposing under visible-light irradiation Bi_2O_3 semiconductor possesses good electron (e−) conduction ability. On the other hand, TiO_2 has a loosely packed structure as well as higher degree of openness, which favors the hole (h+) transport in the crystal lattice by the available displacement of the oxygen atoms through the strong vibration model (associated with O-). Thus, in such a heterojunction system, one component, Bi_2O_3 of the composite with fair electron (e-) conductivity cooperates with a semiconducting material, TiO_2 with an open structure and the fair mobility for the hole (h+) conduction. Hence, when Bi_2O_3/TiO_2 heterojunction is formed, the inner electric field will be established in the interface. The photogenerated electron-hole pairs will be separated effectively by the inner electric field, and the photocatalytic activity is enhanced. Such a phenomenon gives us an implication for a design scheme for the efficient heterojunction photocatalysts between Bi_2O_3 and TiO_2.

In our study, we have developed a series of heterojunction Bi_2O_3/TiO_2. The prepared Bi_2O_3/TiO_2 nanoheterojunction was applied to the photocatalytic degradation of ROC. The composite Bi_2O_3/TiO_2 demonstrated enhanced photocatalytic efficiency compare to that of Bi_2O_3 and Degussa P25 under-visible light irradiation.

Chapter 2 Materials and Methodology

The objective of our research was to study fabrication of Bi_2O_3/TiO_2 heterojunction nanocomposites and their applications to the degradation of pollutants in water, thus, first and foremost was the synthesis of nanostructured photo-catalysts. The principle of the synthesis method is as follows: Couple TiO_2 (wide band gap) with Bi_2O_3 (narrow band gap) semiconductors to extend the light absorbing property in order to enhance its photo-catalytic efficiency (Tarabanov, 1992; Martin et al., 1997).

Nanostructured photo-catalysts we planed to fabricate mainly contain: TiO_2, Bi_2O_3 and Bi_2O_3/TiO_2 heterojunction nanocomposites at different Bi-Ti atomic ratios. Main methods we taken such as direct hydrolysis, hydrothermal, co-precipitation and so on. By the research, we want to study out in which Bi-Ti ratio the nanocomposite will exhibite high photocatalytic activity.

2.1 Materials

All reagents were purchased from commercial sources and were used as received. The purity of the titanium dioxide (TiO_2) was used in this research was 99% (Merck KGaA, Darmstadt, Germany). All chemicals used in this study are of reagent grade. The water used in the preparation of all the synthetic solutions was from a Millipore Direct-Q water purification system. The ROC (Reverse Osmosis Concentrate) water we used in this experiment was collected

from a waste water treatment plant in Malaysia. Before each experiment, The ROC water was stored in the fridge.

2.2 Methodology

In our research, a series of Bi_2O_3/TiO_2 heterojunction nan-composites photocatalysts have been prepared, for comparison, Bi_2O_3 powder was also fabricated by adopting the method mentioned in this thesis in the absence of TiO_2, pure TiO_2 was also prepared through the same procedure except for addition of the $Bi(NO_3)_3 \cdot 5H_2O$. Degussa P25 was chosen as the standard TiO_2 nanoparticle.

In this experiment, we mainly fabricated inorganic hollow spheres as catalyst, there are some reasons for this. Firstly, big fraction of void space could be used for to load and release small materials. Secondly, low density and high surface area, make them very popular among methods of catalysis synthesizing. Last but not least is that easy accessibility and special capability of obtaining monodispersed products with well-defined morphology,

In brief, in this method, metal ions firstly penetrate into the surface of carbon spheres, in order to remove of carbon cores, calcination of the composite spheres is adopted, leading to the formation of oxide hollow.

2.2.1 Preparation of carbon spheres

The first and crucial step is the preparation of multi-metal oxide hollow sphere

using layered double oxide precursors strategy of preparing oxide hollow spheres. As shown in the Fig.2-1, the main procedures are as follows, the first step is combination, Bi_2O_3/TiO_2 heterojunction nan-composites with the exact ratio were naturally attached to the surface of negatively charged carbon spheres driven by electrostatic force, the next step is calcination, once they were mixed, leading to a coating of Bi_2O_3/TiO_2 on CSs. After the removal of carbon cores by calcination, Layered Double Oxides (multi-metal oxides) with hollow spherical morphology were formed (Matthews, 1984).

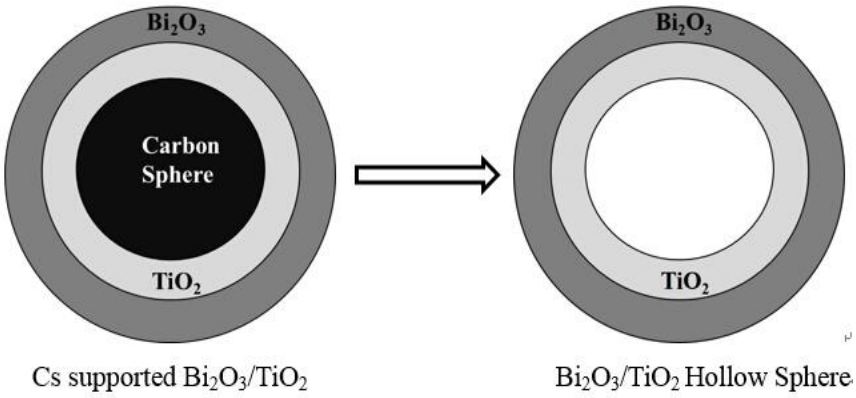

Figure 2-1 Chematic illustration of the formation of Bi_2O_3/TiO_2 heterojunction

As to the Bi-Ti atomic ratio in the mixture was as follows, Bi:Ti=0:100, 5:95, 20:80, 50:50, 80:20, 95:5, 100:0, and the details is shown in the Table.2-1.

Table 2-1 Details on different fabricated Bi_2O_3/TiO_2 heterojunction.

Sample	**Bi n(mmol)**	**Bi mol%**	**Ti mol% Ti**	**Ti n (mmol)**	**（CS）**
C1	0	0	100	6.32	0.50
C2	0.32	5	95	6.00	0.50
C3	1.27	20	80	5.06	0.50
C4	3.16	50	50	3.16	0.50
C5	5.06	80	20	1.27	0.50
C6	6.00	95	5	0.32	0.50
C7	6.32	100	0	0	0.50

Therefore, heterojunction nanocomposites photocatalysts Bi_2O_3/TiO_2 were prepared by combining two semiconductors Bi_2O_3 and TiO_2 varying the Bi_2O_3/TiO_2 molar ratio. Carbon spheres are employed as an inorganic binder to unite Bi_2O_3 and TiO_2 nanoparticles.

According to related previous reports, carbon spheres were synthesized in a hydrothermal reaction of boric acid and D-glucose, and carbon spheres have homogeneous sizes (Matthews, 1988). Accordingly, the boric acid (2.0 g) and D-glucose (16.0 g) were firstly dissolved in 40 mL deionized water. The aqueous solution was sealed in a Teflon-lined stainless steel autoclave. The autoclaves were heated to 180℃ and keep the temperature for 6 h under autogenously pressure, and air cooled down to room temperature. After that, the

resulting products were collected and centrifuged, and then, washed with deionized water for two times and anhydrous ethanol for one time, and dried at 60 ℃ in an oven overnight.

Figure 2-2 Synthesized carbon spheres

2.2.2 Preparation of carbon sphere supported TiO_2

Table 2-2 The dosages of $Bi(NO_3)_3$•$5H_2O$ and $TiOSO_4$•xH_2O

Sample	$Bi(NO_3)_3$ $5H_2O$ n(mmol)	M(mg)	$TiOSO_4$ ·xH_2O n(mmol)	M(mg)	（CS）
C1	0	0	6.32	2.10	0.50
C2	0.32	0.15	6.00	1.99	0.50
C3	1.27	0.62	5.06	1.68	0.50
C4	3.16	1.53	3.16	1.05	0.50
C5	5.06	2.45	1.27	0.42	0.50
C6	6.00	2.91	0.32	0.11	0.50
C7	6.32	3.07	0	0	0.50

As for this method, the procedures were as follows: 4 g Titanium oxysulfate hydrate ($TiOSO_4$ ·xH_2O) was first added into the reaction kettle, and 80 mL of deionized water was then added into the reaction kettle in a fume hood, 20 mL ethanol was then added into the vessel. The solution was stirred and reaction was allowed to proceed at room temperature, when the solution turned to colorless, added 0.5g carbon spheres into the solution and the reaction was allowed to proceed at 90 ℃ for 6 h (Fig.2-3). After reaction, the kettle was cooled down to room temperature, and got Static hierarchical overnight. And then made a centrifugal separation, washed the sediment with Ammonia until the range of PH was 5~7. The main reaction was (Ohno et al., 2003):

$$TiOSO_4+H_2O\rightarrow Ti(OH)_4+H_2SO_4.$$

Figure 2-3 Schematic of photoreactor used in this study

2.2.3 Fabrication of Bi_2O_3 /TiO_2

Bi_2O_3 powder was prepared according to the following process.weighed 1.54g Bismuth trinitrate pentahydrate ($Bi(NO_3)_3$ $5H_2O$), added into deionized water，added Nitric(65%) acid into solution，got water bath heating at 50℃. Until all the samples dissolved, when the kettle was cooled down to room temperature, added C-supported TiO_2 into the liquor, and stirred the mixed liquid for 30 mins. Added the ammonia solution dropwise into into the vessel, stirred the solution, until the pH was in the range of 5~7. Then keep the mixed liquid Aging more than 2h, got out the upper layer, and made centrifugal separation (13000 r/min for 2mins) to the residue and washed for 3 times. Dried the sample at 60℃ (overnight. Finally, calcined the sample at 600℃ for 1h.

Another Bi_2O_3/TiO_2 heterojunction nanocomposites, Bi : Ti atomic ratios as: 0:100, 5:95, 20:80, 50:50, 80:20, 95:5, 100:0 synthesized following the same procedure. For purpose of comparison, commercial TiO_2 purchased from Sigma-Aldrich (99.9 %) was also used.

Figure 2-4 Synthesized Bi_2O_3/TiO_2 heterojunction nanocomposites.

As shown in the figure, Bi_2O_3/TiO_2 heterojunction nanocomposites synthesised are mainly white or yellow powders.

2.3 Characterization

Many analytical techniques were used to characterize the photocatalysts. The most important characterization techniques used in the preparation of this thesis include powder X-ray diffraction (XRD), nitrogen sorption porosimetry, scanning electron microscopy (SEM), UV-vis molecular absorption spectroscopy, UV-Vis diffuse reflectance spectroscopy (DRS), and fluorescence spectroscopy (Wilson et al., 2002).

2.3.1 Powder X-ray Diffraction

Powder X-ray diffraction is used to identify bulk phases, to quantify the different phases in the photocatalysts, and to estimate the average crystallite size of the nanoparticles. The formation of Bi_2O_3/TiO_2 heterojunction

nanocomposites structure were confirmed by XRD (x-ray diffraction) patterns. A powder diffractometer D5005 (Simens, Germany) equipped with a Cu Kα radiation source was used in this experiment. The accelerating voltage was 40 kV and current was 40 mA, respectively. The scanning range of 2θ for MCM-41 confirmation was from 1.4 to 9 °, with a step size of 0.02 °/s. While the scanning range of 2θ for fly ash was from 5 to 70 °, with a step size of 0.04 °/s.

When the sample is irradiated with monochromatic X-rays, the X-rays are diffracted by the network of atoms within the crystal structure and beams reflected in the same direction interact with each other. The resultant amplitude depends on the phase shifts of the waves as they move through different distances and interact with different atoms as they penetrate through the crystal planes. The diffraction angle at which positive interference occurs obeys the Bragg diffraction law (Dinnebier and Billinge, 2008):

$$2d\sin\theta = n\lambda \qquad (2.1)$$

where d is the interplanar distance, θ is the incident angle of x-ray beam, λ is the wavelength of x-ray and n is the integer known as the order of reflection.

The intensity of the peaks depends on the nature of the atoms composing the crystal structure and their relative positions within the lattice cell. Each crystalline solid has its unique characteristic X-ray diffraction pattern that may be used as a “finger print” for comparison. The International Centre for Diffraction Data (ICDD) provides the standard powder diffraction patterns of a large number of compounds in the form of JCPDS cards. The structure of an

unknown compound can be roughly identified by comparing with the data summarized in these cards. Other information such as the space group and crystal structure can also be extracted from the diffractograms.

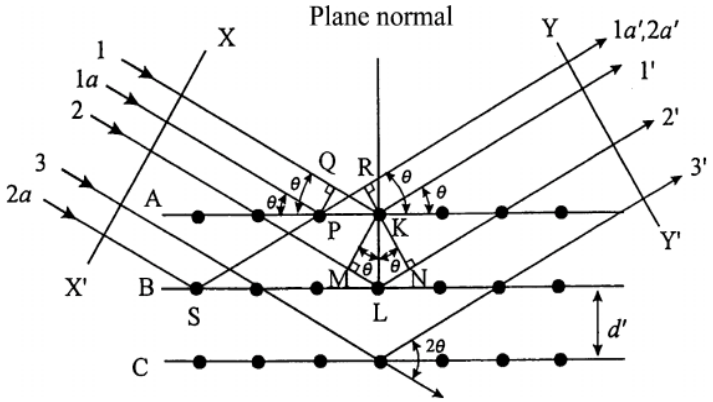

Figure 2-5 Schematic diagram of the scattering of x-rays by a crystalline material (Waseda et al., 2011).

According to the theory of diffraction (Robinson et al., 2004), the pattern of polycrystalline samples consists of sharp lines. However, some degree of broadening of these lines is always presented in practice, which is determined by the crystallite size distribution, the presence, nature and extension of lattice strains, and the spectral distribution of energy. The Scherrer equation relates the size of the crystallites to the broadening of the diffraction peak (Patterson,1939).

$$\tau = \frac{k\lambda}{\beta \cos\theta} \tag{2.2}$$

where τ is the mean crystallite size, k is the dimensionless shape factor with a value close to unity, λ is the wavelength of the x-ray used, β is the (instrumental broadening corrected) peak width at half maximum (FWHM) and θ is the Bragg's angle in radian. In Scherrer's original derivation, it was assumed that

the crystal was cubic and the line profile was approximated by a Gaussian function. The value of k obtained was 0.94. The exact value varies with the actual shape of the crystallites, but an average value of 0.9 is used in most cases. This equation is only applicable to nanoscale particles and cannot be used on samples with crystallite size larger than 0.1 μm.

In this study, XRD measurements were made using a Siemens 5005 diffractometer which is a θ-θ system and using Ni-filtered Cu-Kα X-ray radiation (λ = 1.54056Å). The peak line width β was corrected for the instrumental broadening, using the formula $\beta = \sqrt{B^2 - b^2}$. B is the measured peak width and b is the instrumental broadening, determined from the line width of a well crystallized quartz material.

2.3.2 BET analysis

BET method from the linear part of BET plot (IUPAC recommendation), which use the relative pressure (p/p0) = 0.05- 0.23 adsorption isotherm was performed to calculate the specific area. The porous properties were examined by N_2 adsorption and desorption isotherms at 77 K, using an ASAP 2020 (Micromeritics, American) instruments. BJH method was used to investigate the pore size distribution and the pore volume was obtained from the maximum amount of adsorption at p/p_0 of 0.99. Before analysis, the samples were degased at 110 ℃ under liquid nitrogen condition for nearly 8 hours.

2.3.3 N_2 sorption porosimetry

In order to measure the surface area of the solid photocatalysts, The N_2 sorption technique is used. Molecules of N_2 are physically adsorbed under controlled condition within a vacuum chamber at its boiling point temperature 77.35 K. The adsorption takes place on the entire particle surface, including the external and internal pore surfaces. An N_2 adsorption/desorption isotherm can be obtained by measuring the pressure of the gas above the sample as a function of the volume of gas introduced into the chamber. The surface area can be calculated from this isotherm by Brunauer-Emmett-Teller (BET) theory [6].

Physisorption occurs when weak and long range Van der Waal's forces of attraction are formed between the gas adsorbate and the solid surface. This type of adsorption is fairly material-independent and takes place between all gas molecules on any surface at sufficiently low temperatures. The Langmuir isotherm models simple monolayer adsorption equilibrium. However, it is observed in most cases that the amount of adsorption increases infinitely as pressure increases. In 1930's, Brunauer-Emmett-Teller (BET) extended Langmuir's theory to the multilayer adsorption (Brunauer et al., 1938). The mathematical expression of the multi-layer adsorption is as follows:

$$\theta = \frac{v}{v_m} = \frac{c\frac{P}{P_o}}{(1-\frac{P}{P_o})[1-\frac{P}{P_o}(1-c)]} \qquad (2.3)$$

where θ = coverage (no. of occupied sites/ total no. of possible sites), v = total

volume adsorbed, v_m = volume for monolayer coverage, P = equilibrium pressure, P_o = saturation pressure of the adsorbate at the temperature of adsorption and c = BET constant which can be expressed as:

$$c = \exp\left(\frac{E_{ADS} - E_{COND}}{RT}\right) \tag{2.4}$$

where E_{ADS} = heat of adsorption for first layer, E_{COND} = heat of adsorption for second and higher layer = heat of condensation

Total surface area $S_{BET,T}$ and specific surface area S_{BET} in m^2/g can then be evaluated using the following equations:

$$S_{BET,T} = \frac{(v_m N s)}{V} \tag{2.6}$$

$$S_{BET} = \frac{S_{BET,T}}{a} \tag{2.7}$$

where N = Avogadro's number, s = adsorption cross-section area of the adsorbate molecule (N_2 = 16.2 $Å^2$/molecule), V = molar volume of gas adsorbate, a = mass of sample (in grams).

The BET method is the most popular means of measuring surface areas of finely divided solids. It is reproducible and easily to perform. But it does have some serious limitations (Morel, 1990). Since a heating and degassing procedure is required, it is not applicable for solids that interact strongly with water. By using nitrogen molecules as adsorbents, it cannot detect pores that are smaller than the dinitrogen molecule. The accuracy of BET measurements depends on the validity of the assumptions underlying the data analysis method. In this thesis, the BET method is adoptable.

In our experiment, the surface area of the photocatalysts was determined by a micromeritics tristar 3000 instrument. The powdered samples (0.1 g- 0.15 g) were degassed in a sample tube with a slow flow of N_2 for approximately 5 h at 300 ^oC for those samples calcined higher than 300 ^oC, and at 100 ^oC for those samples treated below 300 ^oC in the sample preparation, in order to remove any water and contaminants present on the surface. After degassing, the sample was accurately weighted and sample tubes containing the samples were connected to the analysis port of BET instrument. During measurements, the sample tubes were immersed in a dewar containing liquid nitrogen to maintain it at a constant temperature. Gaseous nitrogen was introduced in small doses under instrument control, and the adsorption/desorption process was followed by measuring the amount of gas adsorbed at various N_2 partial pressure.

2.3.4 Scanning electron microscopy

The scanning electron microscopy (SEM) is an instrument that produces high resolution images by using electrons instead of light to form an image (Niemantsverdriet, 2008). SEM images have a characteristic three-dimensional appearance and are used to judge the surface structure of the sample.

In the scanning electron microscope, a beam of electrons is generated in a vacuum. This electron beam is focused into a fine probe and subsequently raster scanned over a small rectangular area of a sample. As the beam interacts with the sample, it creates various signals (secondary electrons, internal currents,

photon emissions, etc.). These secondary electrons are detected by a scintillation material that produces a flash of light for each electron. The light flashes are then detected and amplified by a photomultiplier tube. By correlating the sample scan position with the resulting signal, an image can be formed. The illumination and shadowing shows a quite natural looking surface topography.

In this study, the SEM was used to study the topography and morphology of the photocatalysts. The low resolution SEM images were obtained on a JEOL JSM-5200 microscope using 15 kV or 20 kV electron beams, while the high resolution SEM images were obtained on a JEOL JSM-6701F SEM (field-emission) with voltage of 5 kV.

2.3.5 UV-vis diffuse reflectance spectroscopy

UV-vis diffuse reflectance spectroscopy is a useful spectroscopic technique based on the reflection of light in the UV and visible region by a powdered sample that probes the absorption of light and band gap energy of the photocatalysts.The illumination of powdered samples by incident radiation leads to diffuse illumination of the samples. The incident light is partially absorbed, partially scattered. The scattered radiation, emanating from the sample is collected in an integration sphere and detected.

The band gap of semiconductor photocatalysts, which is defined as the minimum photon energy required to excite an electron from the highest occupied molecular orbital to the lowest unoccupied molecular orbital, can be

obtained from the diffuse reflectance UV-vis absorption spectra. There are two basic types of electronic transitions, namely direct transitions and indirect transitions. Direct transitions require only that photons excite electrons, while indirect transitions also require concerted vibrations and energy from the crystal lattice (phonons). The energy dependence of the absorption coefficient (R) for semiconductors in the region near the absorption edge is given by

In this work, the diffuse reflectance spectra were taken using a Shimadzu UV-2450 UV-Visible spectrophotometer with diffuse reflectance accessory ISR-240A. $BaSO_4$ was used as the reference. The band gaps were obtained from plots of $(F(R\infty)\bullet h\nu)^{1/2}$ versus the energy of light for direct band gap semiconductors or the plot of $(F(R\infty)\bullet h\nu)^2$ versus the energy of light for indirect band gap semiconductors.

2.2.6 Fluorescence spectroscopy

Fluorescence spectroscopy is primarily concerned with electronic and vibrational states. Fluorescence spectroscopy is a type of electromagnetic spectroscopy can analyze fluorescence from a sample. By absorbing a photon, the species is excited from its ground electronic state to one of the various vibrational states in the excited electronic state.

It is possible to record both emission and excitation spectra with most spectrofluorometers. An emission spectrum is the wavelength distribution of an emission measured at a single constant excitation wavelength, while an

excitation spectrum is the dependence of emission intensity, measured at a single emission wavelength, on scanning the excitation wavelength.

2.3.7 TOC analysis

TOC-VWS (Shimadzu, Japan) was used to detect organic compounds variation of ROC. TOC analysis method which used O_2 to oxidize organics at a high temperature can efficiently detect hard to decompose, insoluble and macromolecular organic compounds, not just easily decomposed, low molecular weight compounds. This TOC detection machine has high sensibility whose detection limit can reach ppb level, thus is fit for reverse osmosis concentrate detection.

Chapter 3 Results and discussion

3.1 XRD analysis

As we known that, different substances have different X-ray diffraction patterns, while the same substance always shows the same pattern. In a mixture of different substances, each kind of matter produces the same crystalline pattern independently from others. In our experiment, a series of Bi_2O_3/TiO_2 samples with different Bi: Ti ratio was prepared.

X-ray diffraction (XRD) studies were taken practice in 2θ range of 20-80 °using an X-ray diffractometer. The XRD patterns were analyzed by matching the observed peaks with the standard pattern provided by JCPDS file (Ramsden, 1996). According to x-ray diffraction data (Fig.3-1), the phase composition of the Bi_2O_3/TiO_2 materials depends on Bi_2O_3 content. It shows the XRD patterns of TiO_2, Bi_2O_3 and Bi_2O_3/TiO_2 composites with different bismuth contents.The X-ray diffraction patterns of pure Bi_2O_3 and TiO_2 agreed well with the patterns of α-Bi_2O_3 (JPCDS No.65-2366) and TiO_2 (JPCDS No.06-0249), respectively. In the heterojunction, the TiO_2 in the photocatalysts was in anatase phase and the Bi_2O_3 was in alpha phase when Bi:Ti molar ratios were at 100:0 or less than 50:50 (5:95; 20:80). However, when Bi molar ratios were increased to > 50:50 (95:5; 80:20; 50:50), an unidentified phase appeared which could be $Ti_3(BiO_3)_4$ or other titanium bismuthate compounds.

XRD peaks at 2θ=25.28 °and 2θ=27.40 ° are usually regarded as the

characteristic peaks of anatase (101) and rutile (110) crystal phase, respectively. From fig.3-1, it can be noted that pure TiO_2 (Bi:Ti=0:100) have important diffraction peaks around 2θ of 25.3, 37.8, 47.8, 53.8, 55.0, 62.1, 62.7, 68.8, 70.3, and 75.0 respectively, these peaks represent the characteristic of anatase phase. However, there were also rutile detected, meaning that there is some phase transformation in experimental conditions. It is observed that Bi_2O_3/TiO_2 (Bi:Ti=20:80) exhibits a coexistence of both Bi_2O_3 and TiO_2 phases, Compared with pure TiO_2, Another Bi_2O_3/TiO_2 heterojunction nanocomposites exhibit no rutile characteristic peak. From these results, we can conclude that, the surface-modification with Bi can inhibit effectively the phase transformation from anatase to rutile, which is favorable to the improvement of the anatase crystallinity. The high crystallization degree of anatase facilitates the rapid transform of photoelectrons from bulk to the surface, which could inhibit the recombination effectively between holes and photoelectrons, leading to enhanced efficiency of photocatalytic quantum. However, the crystallization degree and sizes of Bi_2O_3/TiO_2 decrease slightly with the increase of bismuth contents, as mainly evidenced by the intensity and the full width at the half maximum (FWHM) values of their characteristic XRD peaks (Huang, 2013). The reason may be that the presence of bismuth disturbs the crystallization process during calcination.

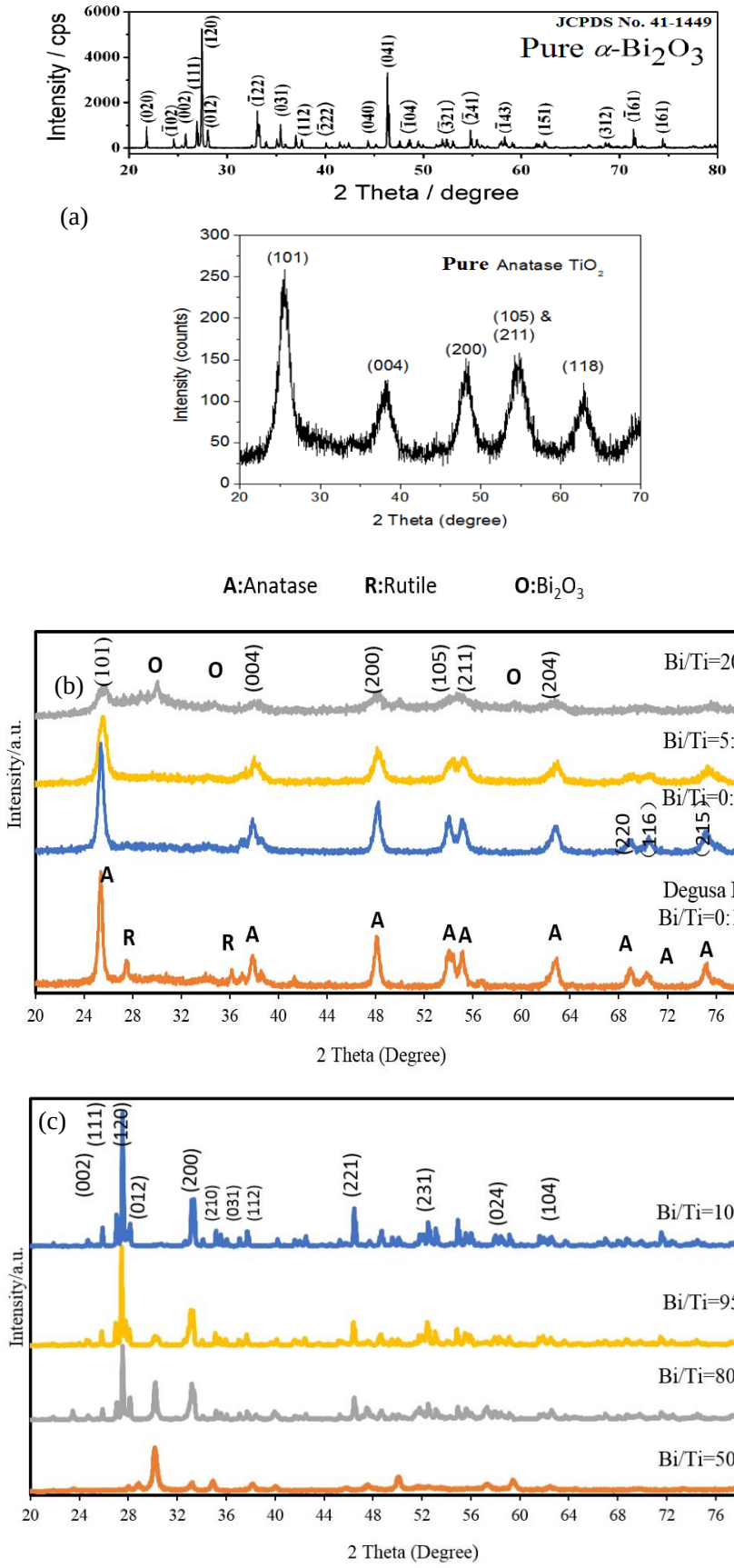

Figure 3-1 The X-ray powder diffraction patterns of pure α - Bi_2O_3 and TiO_2 (a), Bi_2O_3/TiO_2 photocatalysts(b,c)

3.2 FT-IR analysis

FTIR spectroscopy was useful technique to confirm the results concerning the identification of the bismuth oxide phases given by the XRD pattern. In our experiment, Fourier transform infrared (FTIR) spectra were acquired by use of the KBr method on an FTIR spectrometer. The surface hydroxyl groups on titania have been recognized to play an important role on the photocatalytic reaction (He, 2014).

Fig.3-2. shows the FTIR spectra of different TiO_2 samples diluted and pressed in KBr dics. As shown in Fig. 4. The spectra showed a strong absorption band in the 544.00-424.00 cm^{-1} range. It is owing to Bi-O stretching mode. This phenomenon is in accordance with data studied by Xie et al (2014), they showed that in the range of 600.00-400.00 cm^{-1}, the deformation and stretching modes involving Bi-O modes are found. Yu et al (2005) also proved that considered the intensity and the mean wavenumber of the bands, absorption bands found in the range 800.00-200.00 cm^{-1} can be related to the stretching mode vibration of each type of Bi-O. The absorption band at 424.00, 508.00 and 544.00 cm^{-1} in FTIR spectra are signed to α-Bi_2O_3 (Shenawi-khalil et al., 2002). These findings are in agreement with XRD diffractogram results discussed earlier. Thus, very pure samples can be obtained from precipitation method and followed later by thermal treatment.

The strong and broad IR band of curve a and b between 400~850 cm^{-1} correspond to the Ti-O stretching vibration modes in crystal TiO_2 With the

increase in bismuth content, the additional peak around 489 cm^{-1} appears due to the vibrations from Bi-O bonds, as displayed in curves. The IR peak at 1630 cm^{-1} is ascribed to the bending vibration of O-H bonds of adsorbed water strongly bound to the catalyst surface.The broad absorption peaks near 3400 cm^{-1} are attributed to the stretching mode of O-H bond, which is related to water molecules and crystal surface hydrogen bonding. Obviously, as the bismuth content of modified TiO_2 samples increases, the amount of surface hydroxyl gradually increases. The larger surface hydroxyl group density will lead to the enhancement of the photocatalytic activity. Because the larger surface hydroxyl group can interact with photogenerated holes, giving better charge transfer and inhibiting the recombination of electron-hole pairs.

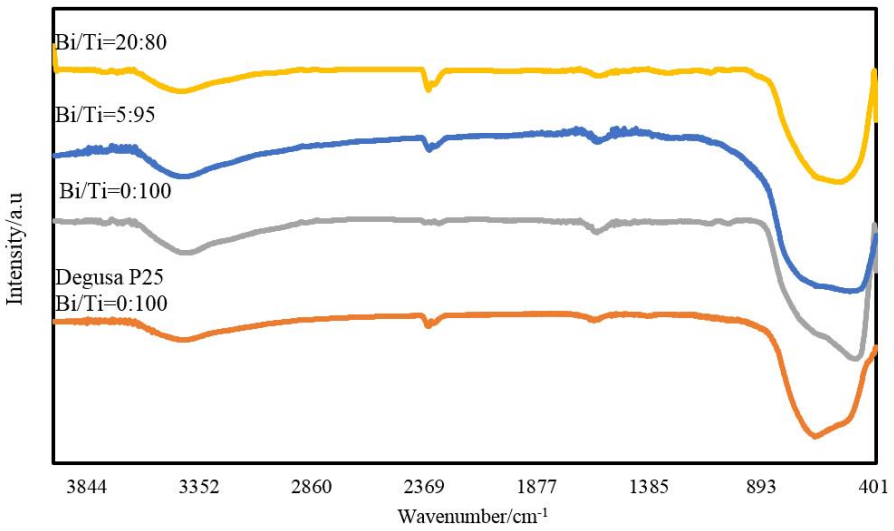

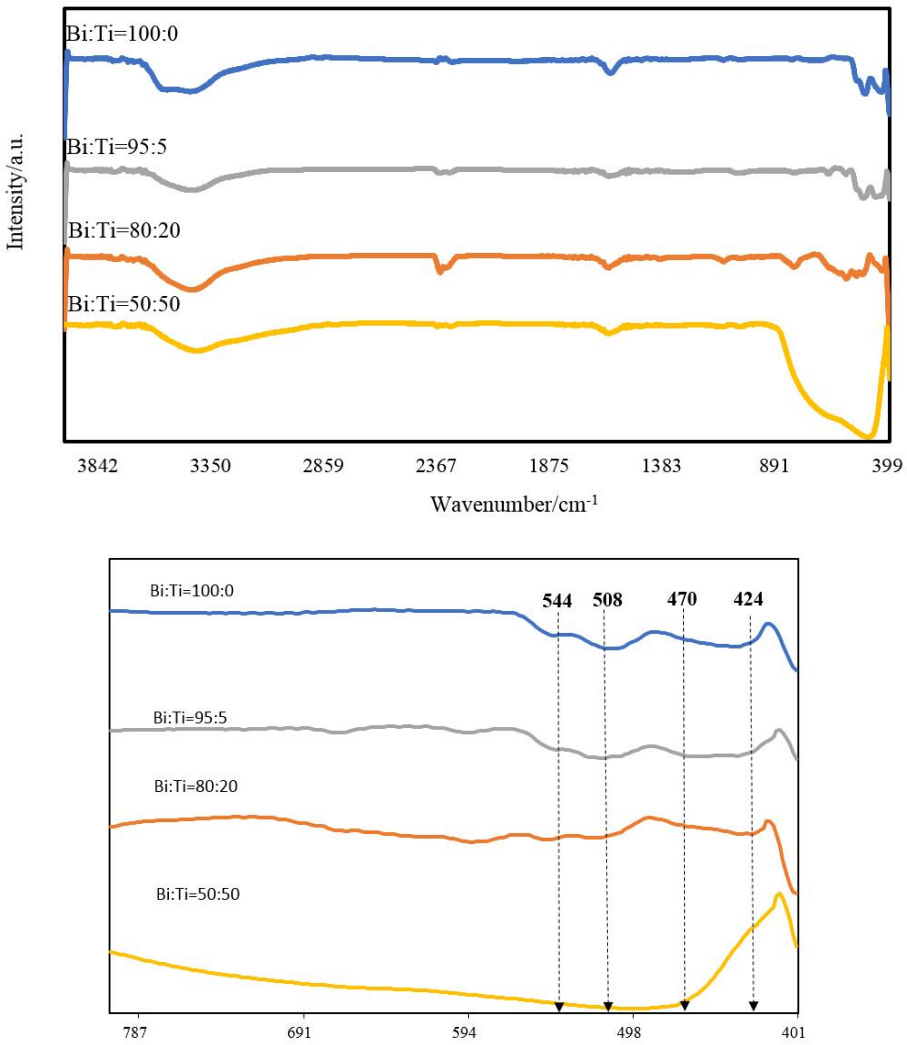

Figure 3-2 FT-IR of Bi_2O_3/TiO_2 heterojunction nanocomposites.

Taking into account the intensity and the mean wavenumber of the bands. The absorption band at 424.00, 508.00 and 544.00 cm^{-1} in FTIR spectra are signed to α-Bi_2O_3.

3.3 BET analysis

BET (Brunauer-Emmett -Teller) method mainly be used to measure the physical adsorption of gas molecules on a solid surface, and can also be used to investigate the specific surface area of a material. The BET surface area was

determined by nitrogen adsorption–desorption isotherm measurements at 77 K by use of a Tristar 3000 micromeritics.The nitrogen adsorption–desorption isotherm of Bi_2O_3/TiO_2 is shown in Fig. 3-3. It is a Type IV sorption isotherm with a hysteresis loop, implying the existence of welldeveloped mesopores in their assembled frameworks (Bahnemann et al., 2007). Usually, the smaller the crystallite size, the larger the specific surface area

In order to study the physical and chemical properties of the surface of the fabricated composite materials, N_2 adsorption–desorption measurement was carried out.

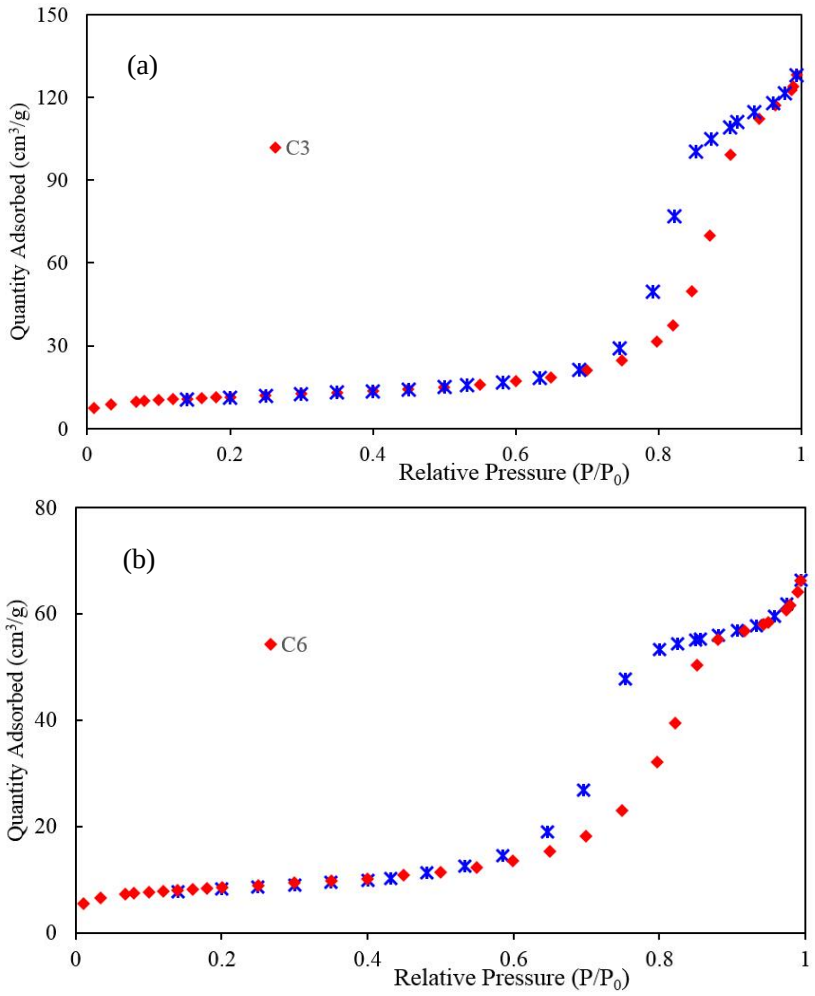

Figure 3-3 Nitrogen adsorption-desorption isotherms of Bi_2O_3/TiO_2, when Bi:Ti molar ratios at 20:80(a), 95:5(b).

As showed in Fig 3-3, nitrogen adsorption-desorption isotherm exhibits a type IV pattern curves, representing the existence of the mesoporous structure according to IUPAC (International Union of Pure and Applied Chemistry) classification. The mesoporous structure was attributed to the holes on the wall of the Bi_2O_3/TiO_2 composite and particle aggregation of Bi_2O_3/TiO_2, respectively. The BET surface areas and pore volumes of both the composites are listed in Table3-1.

Table 3-1 Specific surface and pore architecture of Bi_2O_3/TiO_2 composites

Samples	P25	TiO_2[a]	C1	C2	C3	C4	C5	C6	C7	Bi_2O_3[b]
Bi:Ti	0:100	0:100	0:100	5:95	20:80	50:50	80:20	95:5	100:0	100:0
S_{BET} (m^2g^{-1})	30.72	146.90	29.80	40.15	48.72	2.47	0.66	0.18	0.58	0.45
V_{BJH}(cm^3g^{-1})	0.215	0.100	0.103	0.199	0.329	0.07	0.005	0.001	0.003	0.002

Notes: a – pure anatase TiO_2; b – pure α-Bi_2O_3.

3.4 SEM analysis

The SEM images of different Bi concentration samples are recorded in Fig.3-4. It shows that there is no agglomeration of TiO_2 particles in the matrix, and there is a uniform distribution of the TiO_2 particles in the matrix. According to the SEM images, it was considered that the nanostructured TiO_2 particles are highly microporous, inserted within the netlike structure were built by chains. It notes that the composite is able to extend the liquid-solid interfacial area, and provides a path for the extraction and insertion of ions, and ensures a high reaction rate

(Gospodinova et al., 1998).

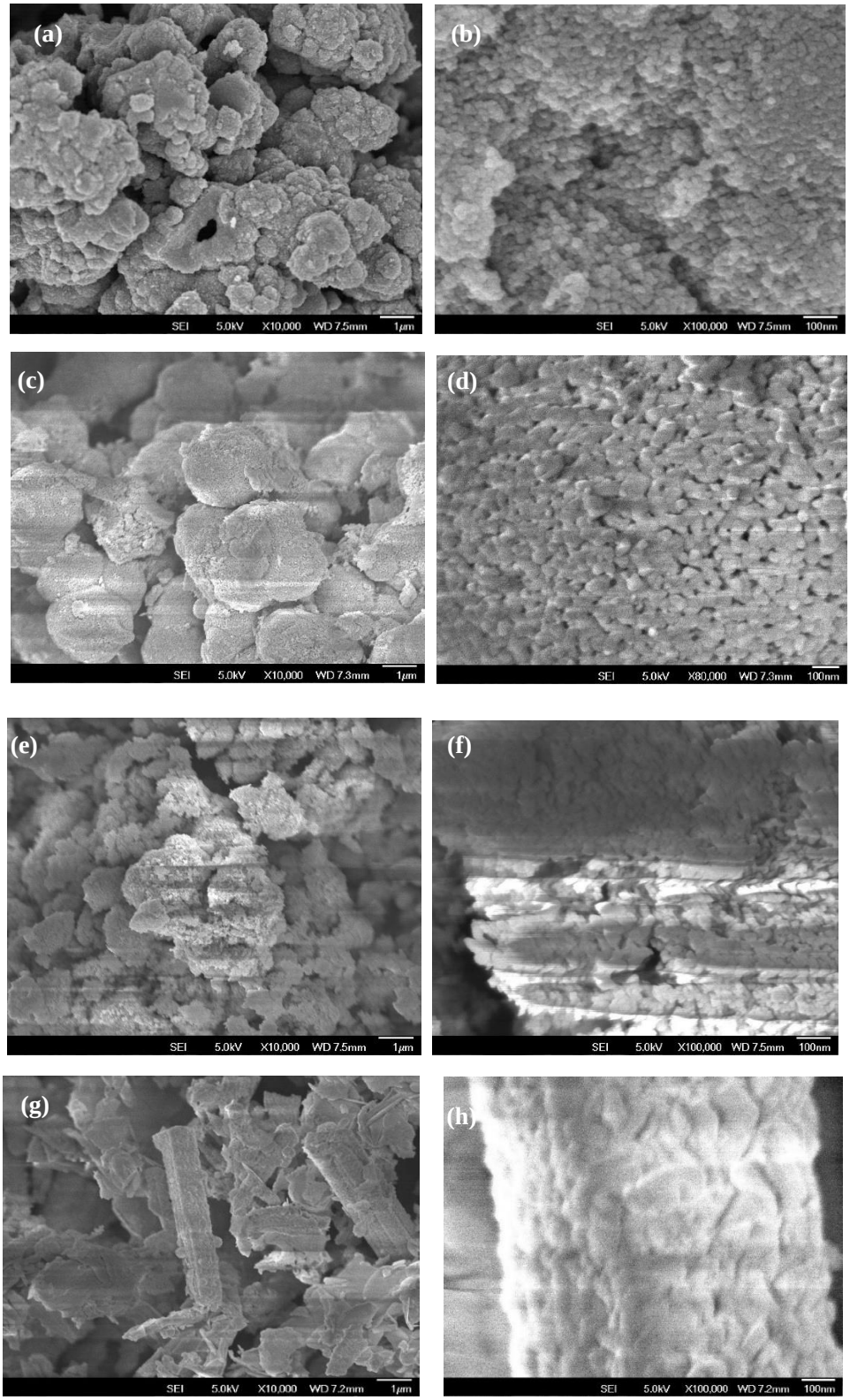

Figure 3-4 SEM of Bi_2O_3/TiO_2 photocatalysts: Bi:Ti molar ratios at 0:100(a,b), 50:50(c,d) , 20:80(e,f) ,80:20(g,h)

3.5 UV–visible DRS analysis

UV–visible diffuse reflectance spectra (DRS) in the wavelength range 200-800 nm were recorded by use of a Shimadzu UV-2550 spectrophotometer with $BaSO_4$ as reference.Figure 5 shows the optical properties of TiO_2 and Bi_2O_3/TiO_2, which were measured by UV–visible DRS. For large energy gap of anatase (3.2 eV) TiO_2 has almost no significant absorbance in the visible light region. By comparison, reflection by Bi_2O_3/TiO_2 was much less (i.e. more light was absorbed) for wavelengths from 390 to 700 nm; this was attributed to the presence of Bi_2O_3 with a narrow energy band gap (2.8 eV). The absorption spectra of Bi_2O_3/TiO_2 extended to larger wavelength so that lower-energy photons could be absorbed for photoreaction; this was indicative of efficient utilization of visible light for photocatalytic degradation.

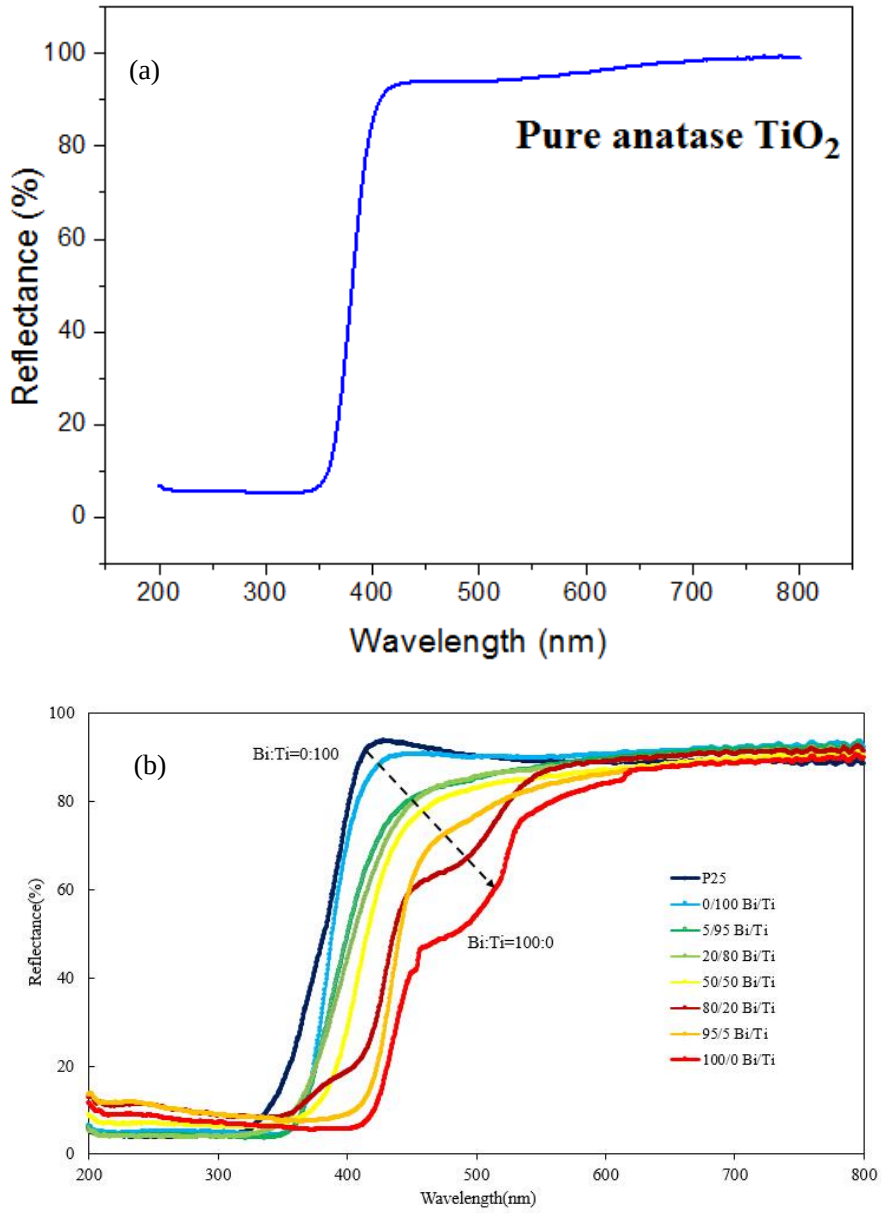

Figure 3-5 UV-Visible diffuse reflectance spectra of pure anatase TiO_2 (a) and Bi_2O_3/TiO_2 heterojunction (b).

As shown in Fig.3-5, the UV-Vis DRS spectra demonstrate that the pure TiO_2 displays no significant absorbance in the visible region due to the big ennergy gap (3.2 eV). With the introduction of Bi ions, the absorption edge shifts towards longer wavelengths (400~600 nm). The absorbance of Bi_2O_3/TiO_2 has similar intensity with the Bi content from 0.5%~2.0%. Meanwhile, further increase of the Bi content is beneficial to the light absorbance. The absorbance

of Bi_2O_3/TiO_2 increase with the Bi content, suggesting that the spectral response in the visible region mainly results from Bi_2O_3/TiO_2 photosensitization (Li et al., 2012).

Briefly, the Bi_2O_3 photo sensitizer with narrow ennergy gap (2.8 eV) could be easily activated by visible lights and induce photoelectrons and holes. The photo-holes in bismuth oxide could easily transfer from the valence band (VB) of Bi_2O_3 to the neighboring VB of TiO_2 (Chen et al., 2012). Thus, the Bi-Ti heterojunctions formed in the composite TiO_2 could effectively inhibit the recombination between photoelectrons and holes, leading to thestrong response in visible area.

Chapter 4 Photo-catalysis Reaction to Degrade ROC

4.1 Photocatalytic experiments

In order to evaluate the photocatalytic activity of the prepared catalysts and find out the optimum content of Bi species, a set of experiments for ROC (Reverse Osmosis Concentrate).

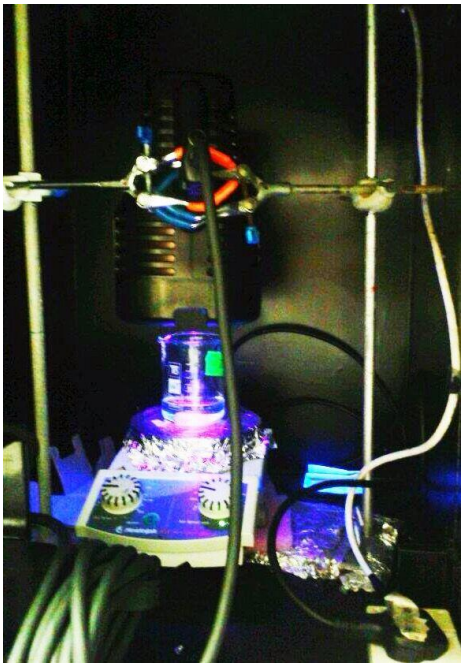

Figure 4-1 Reaction equipment for ROC reaction.

The experimental vessel is depicted in Fig 4-1, the series of catalyst fabricated was used to degrade ROC water. The details of dosage were as follows, 50mL ROC water was treated with 50 mg catalyst. The wavelength of the UV lamp we used was 365 nm, and light intensity was about 18 mW/cm^2. For each experiment, stirred the solution for 3 mins in the darkness before treatment. 6

mL sample was taken after each 1, 2, 4, 6 h reaction. To make the results more comparable, all sampling was conducted under stirring condition, and DI water was added to balance the water loss during reaction.

Comparatively, we also carried out the experiment under a Xenon lamp (visible light with UV cutoff at 420 nm), and the procedure was the same except the light sources.

4.2 fluorescent intensity

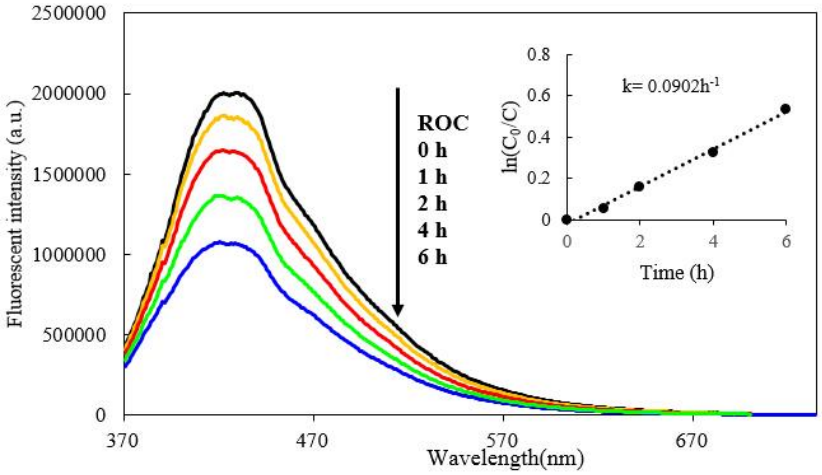

Figure 4-2 Changes in the fluorescent intensity of the RO aqueous solutions under visible light irradiation in the presence of Bi_2O_3/TiO_2 (Bi:Ti=20:80).

Fig. 4-2. Displayed changes in the fluorescent intensity of the RO aqueous solutions under visible light irradiation, it shows that Bi_2O_3/TiO_2 (Bi:Ti=20:80) under visible-light illumination, the fluorescent intensity peak of RO at 430 mm drops rapidly in the presence of Bi_2O_3/TiO_2 NTs. This indicates that the ROC dye is photocatalytically decomposed by Bi_2O_3/TiO_2 NTs. The fluorescent intensity of the dispersion was very low after 6h of irradiation, indicating that a

large proportion of the structure of the dye was destroyed (Zhou et al., 2006).

4.3 Comparison of photocatalytic activities

Degradation under visible light irradiation was carried out, the results are shown in Fig.4-3, the pure TiO_2 is rather inefficient since it could not be activated by visible lights due to a big energy band gap (3.2 eV). Fabrication of TiO_2 with Bi_2O_3 results in abrupt increase of the photocatalytic activity owing to the Bi_2O_3-photosensitization (Chakraborty et al., 2011).

The results of Fig.4-3 show that the effectiveness of the catalyst is strongly dependent on the amount of dopant ions. The ROC degradation efficiency after 6 h follows the order in the figure, the Bi_2O_3/TiO_2 (20/80 Bi/Ti) heterojunction showed the best catalytic efficiency, while P25 and Bi_2O_3/TiO_2 (100/0 Bi/Ti) catalyst displayed the worst. The results are also related to BET specific surface area Bi-modified TiO_2. For instance, the larger the specific surface area provides larger contact area and will lead to higher photo-degradation efficiency. Among the Bi-compounded TiO_2, Bi_2O_3/TiO_2 (20/80 Bi/Ti) catalyst exhibits the highest activity under visible illumination. However, very high Bi content facilitates charge transport and reduces charge recombination and reduce quantum efficiency (Lei et al., 2010).

TiO_2 has high degradation efficiency on ROC (Reverse Osmosis Concentrate). However, TiO_2 is relatively expensive. It's quite necessary to cut down TiO_2 dosage while still keeping its photo-catalytic efficiency (Qourzal et al., 2008).

To reduce the economic cost, in this experiment, TiO_2 was attached onto supporters which have high surface area.

Fig.4-3 shows the comparison of photocatalytic activities of different Bi_2O_3/TiO_2 samples. The photocatalytic activities of Bi_2O_3/TiO_2 (Bi:Ti=20:80) samples on the degradation of ROC under visible light (a) and UV-visible (b) irradiation for various time durations are shown in Fig.4-3. The adsorption ability of the ROC enhanced the contact area between the solution and the catalyst, which in turn also enhanced the photocatalytic activity (Bahnemann et al., 2007). When the catalyst was used in the system, 13.5% of the ROC solution was photodegraded by the Bi_2O_3/TiO_2 (Bi:Ti=20:80) after irradiation for 6 h under visible light. However, during the same irradiation time, only 2.2 % of ROC was photodegraded by the P25. Fig.4-3b shows that a little over 15 % of the ROC was removed by Bi_2O_3/TiO_2 (Bi:Ti=20:80), while, just 2.1% of the ROC was removed by the pure Bi_2O_3.

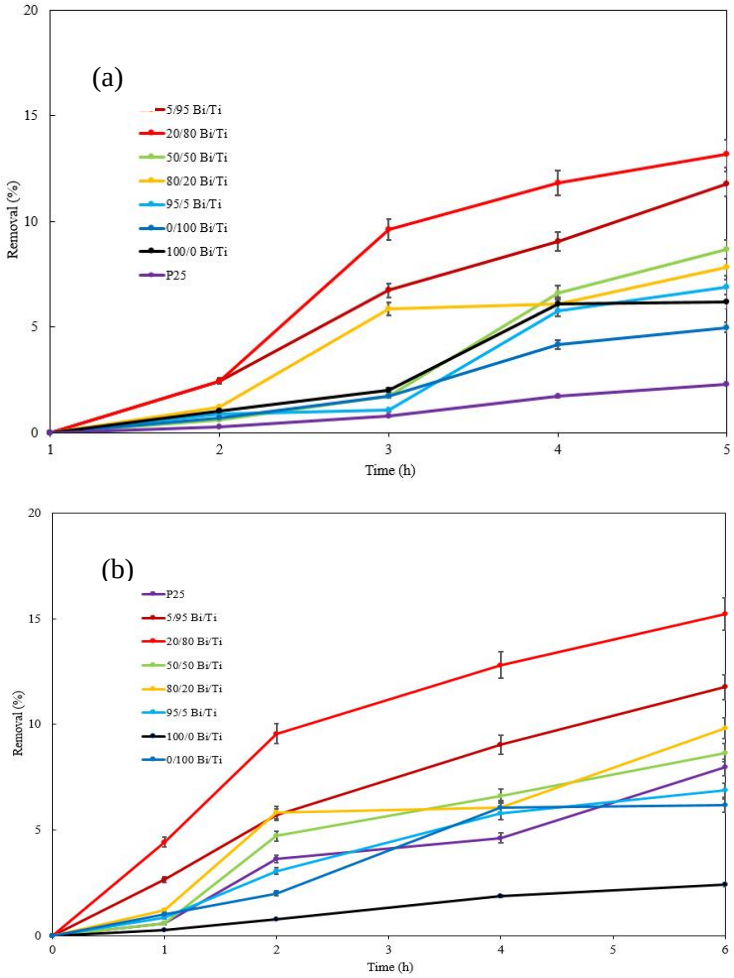

Figure 4-3 Comparison of photocatalytic activities of different Bi_2O_3/TiO_2 NTs for the photocatalytic decomposition of ROC in water under visible-light (a) and UV-light (b).

Therefore, under visible light the activities of heterojunction photocatalysts Bi_2O_3/TiO_2 have been significantly improved from pure anatase TiO_2, Degussa P25 and pure Bi_2O_3. This is manily attributed to the formed B-type heterojunction (Yang et al., 2013; Li et al., 2014) in Bi_2O_3/TiO_2 photocatalysts facilating the e^{-}-h^{+} separation. In such B-type heterojunction Bi_2O_3/TiO_2 (Fig. 4-4) photocatalysts, Bi_2O_3 was activated by visible light due to its narrow bandgap and so electrons were excited to its CB leaving positive holes in its VB. While because of lower energy (higher potential) of Bi_2O_3 VB than TiO_2 VB,

the electrons were transferred from TiO_2 VB to Bi_2O_3 VB resulting in the transfer of positive holes from Bi_2O_3 to TiO_2. So excited electrons were in Bi_2O_3 CB while positive holes were in TiO_2 VB, thus e^--h^+ separation was greatly enhanced. The e^--h^+ separation were crucial to the activity of photocatalysts. However, the definite activities of improved Bi_2O_3/TiO_2 photocatalysts are still not high enough, which could be due to lower surface area, crystalline size, interface charge transfer barrier, and so on. We will continue to optimize the synthesis conditions to further improve the Bi_2O_3/TiO_2 catalysts.

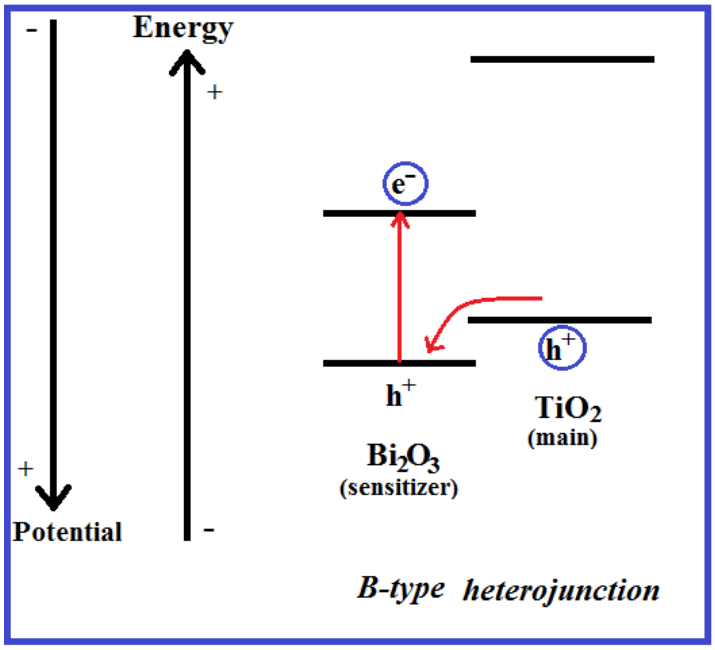

Fig. 4-4 Illustration of formed B-type heterojunction of the Bi_2O_3/TiO_2 photocatalysts.

Chapter 5 Conclusion and future work

A series of Bi_2O_3/TiO_2 heterojunction photocatalysts with different Bi:Ti molar ratios were successfully synthesized using carbon spheres as template and the template was eventually removed leaving the Bi_2O_3/TiO_2 heterojunction photocatalysts untact. Characterization of the Bi_2O_3/TiO_2 heterojunction photocatalysts was done with BET, XRD, SEM, FTIR, and UV-Vis DRS. In the heterojunction, the TiO_2 in the photocatalysts was in anatase phase and the Bi_2O_3 was in alpha phase when Bi:Ti molar ratios were at 100:0 or less than 20:80 (5:95; 20:80). However, when Bi molar ratios were increased to > 50:50 (95:5; 80:20; 50:50), an unidentified phase appeared which could be $Ti_3(BiO_3)_4$, $Ti_2Bi_2O_7$ or other titanium bismuthate compounds. The unidentified titanium bismuthate was also indicated and confirmed by the FTIR peak at 850 cm^{-1}. With low Bi:Ti ratios (0:100 to 20:80), surface area of the Bi_2O_3/TiO_2 heterojunction photocatalysts were still quite high although slightly decreased compared with pure anatase TiO_2 which was in nano-size. But when the Bi:Ti ratios were increased to > 50:50 (100:0; 95:5; 80:20; 50:50), their surface area quickly decreased due to the increase of micron-size Bi_2O_3 platelet and the decrease of nano-size TiO_2 crystallines.

UV-Vis DRS confirmed that with increase of Bi content in the Bi_2O_3/TiO_2 heterojunction photocatalysts their bandgaps decreased so that the wavelength of the visible light they could absorb had red shifts. However, lower bandgaps

did not guarantee the photocatalytic efficiency. Photocatalytic efficiency could be affected by many factors such as suitable bandgap, crystal size, particle size, crystal phase, surface area, surface morphologies, surface species, adsorption site densities, interface charge transfer barrier/speed, e^{-}-h^{+} separation, and so on. In the Bi_2O_3/TiO_2 heterojunction photocatalysts, TiO_2 was the main semiconductor while Bi_2O_3 was the sensitizer and they formed B-type heterojunctions. The formed B-type heterojunction in Bi_2O_3/TiO_2 photocatalysts facilating the e^{-}-h^{+} separation. In such B-type heterojunction Bi_2O_3/TiO_2 photocatalysts, Bi_2O_3 was activated by visible light due to its narrow bandgap and so electrons were excited to its CB leaving positive holes in its VB. While because of lower energy (higher potential) of Bi_2O_3 VB than TiO_2 VB, the electrons were transferred from TiO_2 VB to Bi_2O_3 VB resulting in the transfer of positive holes from Bi_2O_3 to TiO_2. So excited electrons were in Bi_2O_3 CB while positive holes were in TiO_2 VB, thus e^{-}-h^{+} separation was greatly enhanced. The e^{-}-h^{+} separation were crucial to the activity of photocatalysts. Therefore, under visible light the activities of heterojunction photocatalysts Bi_2O_3/TiO_2 have been significantly improved from pure anatase TiO_2, Degussa P25 and pure Bi_2O_3.

However, the definite activities of improved Bi_2O_3/TiO_2 photocatalysts are still not high enough, which could be due to lower surface area, larger crystalline size, higher interface charge transfer barrier, formation of an unknown titanium

bismuthate phase, and so on. The identified titanium bismuthate phase seems to have low photocatalytic activity, so we will control synthesis conditions (mainly Bi:Ti ratio) to avoid it. We will continue to optimize the synthesis conditions to further improve the Bi_2O_3/TiO_2 catalysts. The parameters to be optimized could be calcination temperature, pH values when Bi_2O_3 precitated on TiO_2, control of Bi:Ti ratio to avoid titanium bismuthate phase with low activity, carbon sphere template ratios, modification of carbon sphere surface to have better coverage of each carbon sphere by TiO_2, modification of TiO_2 surface to lower the charge transfer barrier between the two phases in the heterojunction, and so on.

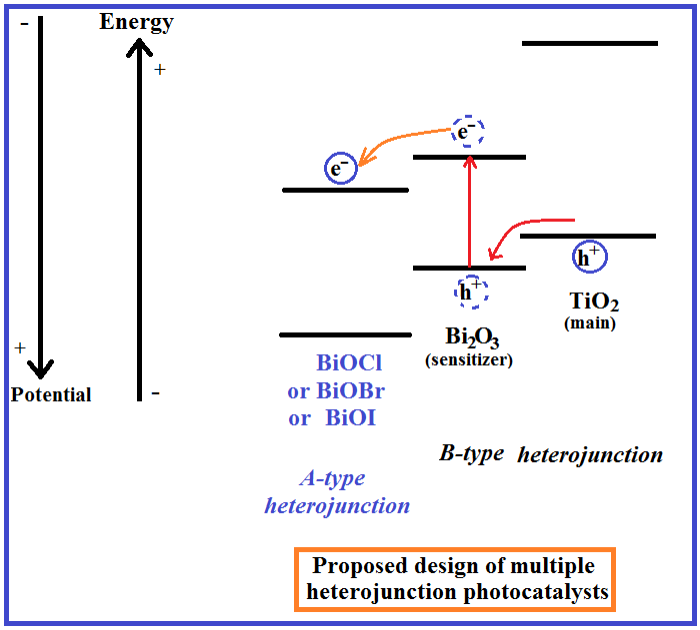

Fig. 5-1 Proposed design of multiple heterojunction photocatalysts with both A-type and B-type heterojunctions in the same catalysts.

Furthermore, a third ingredient (X) could be considered to be added into the Bi_2O_3/TiO_2 heterojunction, forming $X/Bi_2O_3/TiO_2$ multiple heterojunction photocatalysts. Ideally, between X and Bi_2O_3 an A-type heterojunction was formed while a B-type heterojunction was formed between Bi_2O_3 and TiO_2. In such $X/ Bi_2O_3/TiO_2$ multiple heterojunction photocatalysts, excited electrons were transferred to from Bi_2O_3 to X between the X/Bi_2O_3 heterojunction while positive holes were transferred from Bi_2O_3 to TiO_2 between the Bi_2O_3/TiO_2 heterojunction. Such new photocatalysts would be even better e^{-}-h^{+} separation. The new ingredient X could be BiOCl, BiOBr and BiOI which could be achieved by exchanging Bi_2O_3 partially with NaOH forming BiO(OH) and further exchanging with NaCl (NaBr, NaI) to form BiOCl (BiOBr, BiOI). So the eventual new catalysts could be $BiOCl/Bi_2O_3/TiO_2$, $BiOBr/Bi_2O_3/TiO_2$, and $BiOI/Bi_2O_3/TiO_2$. They contained both A-type and B-type heterojunctions, such multiple heterojunctions in a same catalyst are expected to have better separation of electrons and holes to achieve higher photocatalytic efficiency.

REFERENCES

Andreozzi R., M. Canterino, R. Marotta, N. Paxeus, J. Hazard. Mater., 122 (2005) 243-250.

Augugliaro V., V. Loddo, M. Pagliaro, G. Palmisano, L. Palmisano, Clean by Light Irradiation: Practical Applications of Supported TiO_2, Royal Society of Chemistry, 2010. pp 1-40.

Bahnemann W., M. Muneer, M. Haque, Catal. Today, 124 (2007) 133-148.

Bahnemann W., M. Muneer, M. Haque, Catal. Today, 124 (2007) 133-148.

Bi D.F., D.D. Tan, C.Y. Ma, S.H. Xu, in: R. Iranpour, J. Zhao, A. Wang, F.L. Yang, X. Li (Eds.), Advances in Environmental Science and Engineering, Pts 1-6, 2012, pp 720-723.

Brillas, E., I. Sirés, M.A. Oturan, Chem. Rev., 109 (2009) 6570-6631.

Brunauer S., P.H. Emmett, E. Teller, J. Am. Chem. Soc., 60 (1938) 309-319.

Chakraborty A.K., S.B. Rawal, S.Y. Han, S.Y. Chai, W.I. Lee, Appl. Catal. A-Gen., 407 (2011) 217-223.

Chala S., K. Wetchakun, S. Phanichphant, B. Inceesungvorn, N. Wetchakun, J. Alloy. Compd., 597 (2014) 129-135.

Chen L., Q. Zhang, R. Huang, S.-F. Yin, S.-L. Luo, C.-T. Au, Dalton Trans., 41 (2012) 9513-9518.

Choi Y., T. Umebayashi, M. Yoshikawa, J. Mater. Sci., 39 (2004) 1837-1839.

Dinnebier R.E., Billinge S.J.L., Powder Diffraction: Theory and Practice, Royal Society of Chemistry, 2008. pp 1-19.

Dong S.Y., C.F. Yu, Y.K. Li, Y.H. Li, J.H. Sun, X.F. Geng, J. Solid State Chem., 211 (2014) 176-183.

Eberl J., H. Kisch, Photoch. Photobio. Sci., 7 (2008) 1400-1406.

Esplugas S., J. Giménez, S. Contreras, E. Pascual, M. Rodríguez, Water Res., 36 (2002) 1034-1042.

Frame F.A., E.C. Carroll, D.S. Larsen, M. Sarahan, N.D. Browning, F.E.

Osterloh, Chem. Commun., 19 (2008) 2206-2208.

Gospodinova, N., and Terlemezyan, L. Prog. Polym. Sci. 23, 1443 (1998)

He Z.Q., Y.Q. Shi, C. Gao, L.N. Wen, J.M. Chen, S. Song, J. Phys. Chem. C, 118 (2014) 389-398.

Hernandez A M.D., F. Fresno, S. Suarez, J.M. Coronado, Energ. Environ. Sci., 2 (2009) 1231-1257.

Ho W.K., J.C. Yu, J. Mol. Catal. A-Chem., 247 (2006) 268-274.

Hou J.G., R. Cao, S.Q. Jiao, H.M. Zhu, R.V. Kumar, Appl. Catal. B-Environ., 104 (2011) 399-406.

Huang G.F., Z.L. Ma, W.Q. Huang, Y. Tian, C. Jiao, Z.M. Yang, Z. Wan, A.L. Pan, J. Nanomater., 371356 (2013) 1-8

Katsumata H., K. Inoue, T. Suzuki, S. Kaneco, Catal. Lett., 144 (2014) 837-842.

Kim B.H., T.H. Lim, J.W. Roh, S.G. Lee, C.S. Ju, S.S. Park, S.S. Hong, G.D. Lee, React. Kinet. Mech. Cat., 99 (2010) 217-224.

Klavarioti M., D. Mantzavinos, D. Kassinos, Environ. Int., 35 (2009) 402-417.

Kudo A., K. Omori, H. Kato, J. Am. Chem. Soc., 121 (1999) 11459-11467.

Lei Y., G. Wang, S. Song, W. Fan, M. Pang, J. Tang, H. Zhang, Dalton Trans., 39 (2010) 3273-3278.

Leonard N.M., L.C. Wieland, R.S. Mohan, Tetrahedron, 58 (2002) 8373-8397.

Leontie L., M. Caraman, M. Alexe, C. Harnagea, Surf. Sci., 507–510 (2002) 480-485.

Li H.Y., D.J. Wang, P. Wang, H.M. Fan, T.F. Xie, Chem-Eur. J., 15 (2009) 12521-12527.

Li R.G., H.X. Han, F.X. Zhang, D.G. Wang, C. Li, Energ. Environ. Sci., 7 (2014) 1369-1376.

Li X., R. Huang, Y. Hu, Y. Chen, W. Liu, R. Yuan, Z. Li, Inorg. Chem., 51 (2012) 6245-6250.

Li, L., Huang, X. D.; Hu, T. Y.; Wang, J. X.; Zhang, W. Z.; Zhang, J. Q., Synthesis of three-dimensionally ordered macroporous composite Ag/Bi_2O_3-TiO_2 by dual templates and its photocatalytic activities for degradation of organic pollutants under multiple modes. New J. Chem. 2014, 38 (11), 5293-5302.

Liew S.L., Z. Zhang, T.W.G. Goh, G.S. Subramanian, H.L.D. Seng, T.S.A. Hor, H.K. Luo, D.Z. Chi, Int. J. Hydrogen Energ., 39 (2014) 4291-4298.

Lin T., Z. Pi, M.C. Gong, J.B. Zhong, J.L. Wang, Y.Q. Chen, Chinese Chem. Lett., 18 (2007) 241-243.

Martin, C.; G. Solana; V. Rives; G. Marci; L. Palmisano; A. Sclafani. Physicochemical Properties of WO_3/TiO_2 systems employed for 4-nitrophenol photodegradation in aqueous medium. Catal. Lett., 49, pp.235-243. 1997.

Matthews, R. W. Hydroxylation Reactions Induced by Near-ultraviolet Photocatalysis of Aqueous Titanium Dioxide Suspensions. J. Chem. Soc., Faraday Trans., 80, pp.457-471. 1984.

Matthews, R.W. Kinetics of Photocatalytic Oxidation of Organic Solutes over Titanium Dioxide, J. Catal., 111, pp.264-272. 1988.

Morel F. M. M., Surface Complexation Modeling: hydrous Ferric Oxide, John Wiley & Sons, 1990. pp43-45.

Niemantsverdriet J.W., Spectroscopy in Catalysis, Wiley, 2008. pp 167-199.

Ohno, T.; T. Mitsu and M. Matsumura. Photocatalytic Activity of S-doped TiO_2 Photocatalyst under Visible Light, Chem. Lett., 32, pp.364-365. 2003.

Patterson A.L., Phys. Rev., 56 (1939) 978-982.

Pera T M., V. García-Molina, M.A. Baños, J. Giménez, S. Esplugas, Appl. Catal. B-Environ., 47 (2004) 219-256.

Qourzal S., N. Barka, M. Tamimi, A. Assabbane, Y. Ait-Ichou, Appl. Catal. A-Gen., 334 (2008) 386-393.

Ramsden E.N., Detection and Analysis, Nelson Thornes, 1996. pp 52.

Robinson J.W., E.M.S. Frame, G.M. Frame, Undergraduate Instrumental Analysis, Sixth Edition, CRC Press, 2004. pp 535-612.

Serpone N., D. Lawless, R. Khairutdinov, E. Pelizzetti, J. Phys. Chem., 99 (1995) 16655-16661.

Shenawi-khalil S., V. Uvarov, S. Fronton, I. Popov, Y. Sasson, J. Phys. Chem. C, 116 (2012) 11004-11012.

Sheng J.Y., X.J. Li, Y.M. Xu, ACS Catal., 4 (2014) 732-737.

Stepnowski P., A. Zaleska, J. Photoch. Photobio. A, 170 (2005) 45-50.

Tarabanov, G.A., Preparation of TiO2 Ceramics with Bi_2O_3 Additions, Neorg. Mater., 1992, vol. 28, no. 8, pp. 1792–1795.

Thalluri S.M., M. Hussain, G. Saracco, J. Barber, N. Russo, Ind. Eng. Chem. Res., 53 (2014) 2640-2646.

Vogna D., R. Marotta, A. Napolitano, R. Andreozzi, M. d'Ischia, Water Res., 38 (2004) 414-422.

W.F. Yao, H. Wang, X.H. Xu, Y. Zhang, X.N. Yang, S.X. Shang, Y.H. Liu, J.T. Zhou, M. Wang, J. Mol. Catal. A-Chem., 202 (2003) 305-311.

Wang Y., S. Li, X. Xing, F. Huang, Y. Shen, A. Xie, X. Wang, J. Zhang, Chem-Eur. J., 17 (2011) 4802-4808.

Wang Y., Y. Wen, H. Ding, Y. Shan, J. Mater. Sci., 45 (2010) 1385-1392.

Waseda Y., E. Matsubara, K. Shinoda, X-Ray Diffraction Crystallography: Introduction, Examples and Solved Problems, Springer, 2011. pp 74.

Wei J.Y., B.B. Huang, P. Wang, Z.Y. Wang, X.Y. Qin, X.Y. Zhang, X.Y. Jing, H.X. Liu, J.X. Yu, Int. J. Photoenergy, 2012 (2012) 135132.

Wilson J.N., H. Idriss, J. Am. Chem. Soc., 124 (2002) 11284-11285.

Wise D.L., Process Engineering for Pollution Control and Waste Minimization, CRC Press, 1994. pp 363-376.

Xie T.P., L.J. Xu, C.L. Liu, J. Yang, M. Wang, Dalton Trans., 43 (2014) 2211-2220.

Xin J.H., S.M. Zhang, G.D. Qi, X.C. Zheng, W.P. Huang, S.H. Wu, React. Kinet. Catal. L., 86 (2005) 291-298.

Xu C., G.Q. Zhu, J.L. Wu, J. Liang, J. Nanosci. Nanotechno., 14 (2014) 4475-4480.

Xu S.H., W.F. Shangguan, J. Yuan, J.W. Shi, M.X. Chen, Mat. Sci. Eng. B-Solid, 137 (2007) 108-111.

Xu X.H., M. Wang, Y. Hou, W.F. Yao, D. Wang, H. Wang, J. Mater. Sci. Lett., 21 (2002) 1655-1656.

Yang, J.; Dai, J.; Li, J. T., Visible-light-induced photocatalytic reduction of Cr (VI) with coupled Bi2O3/TiO2 photocatalyst and the synergistic bisphenol A oxidation. Environ. Sci. Pollut. Res. 2013, 20 (4), 2435-2447.

Yu Y., C.Y. Cao, H. Liu, P. Li, F.F. Wei, Y. Jiang, W.G. Song, J. Mater. Chem. A, 2 (2014) 1677-1681.

Zhang L.S., W.Z. Wang, J.O. Yang, Z.G. Chen, W.Q. Zhang, L. Zhou, S.W. Liu, Appl. Catal. A-Gen., 308 (2006) 105-110.

Zhang L.S., W.Z. Wang, J.O. Yang, Z.G. Chen, W.Q. Zhang, L. Zhou, S.W. Liu, Appl. Catal. A-Gen., 308 (2006) 105-110.

Zhou J.K., Z.G. Zou, A.K. Ray, X.S. Zhao, Ind. Eng. Chem. Res., 46 (2007) 745-749.

Zhou L., W. Wang, H. Xu, S. Sun, M. Shang, Chem-Eur. J., 15 (2009) 1776-1782.

Zhou L., W. Wang, S. Liu, L. Zhang, H. Xu, W. Zhu, J. Mol. Catal. A-Chem., 252 (2006) 120-124.

Zhu H.J., Q. Li, Nanoscale Res. Lett., 8 (2013) 1-6.